

**University of Warsaw
Faculty of Physics**

Kamil Dutkiewicz
Record book number: 427862

Energy levels in 2D spin dependent optical lattices

Bachelor's thesis
in the field of Physics

The thesis was written under the supervision of
dr Grzegorz Łach
University of Warsaw, Faculty of Physics
Institute of Theoretical Physics

Warsaw, August 2023

Summary

In this study the energy levels of an atom in a 2D spin dependent optical lattice are examined. Expanding upon the work done by P. Szulim *et al.* [2], spin dependence is induced by including a fictitious magnetic field \mathbf{B}_{fic} in the Hamiltonian, apart from the scalar potential. The spectrum of energy levels is analyzed as a function of the external magnetic field \mathbf{B}_{ext} . Wave functions are investigated and used for tracking individual states through varying B_{ext} . Periodic and Dirichlet boundary conditions are considered in both 1 by 1 and 2 by 2 cells. In a 1 by 1 cell the two lowest states' energies intersect for finite value of B_{ext} , while in a 2 by 2 cell avoided crossing occurs but only with Dirichlet boundary conditions. If the laser beams forming the optical lattice are not perpendicular the unit cell of the resulting lattice is a rectangular one. Energy levels are plotted from B_{ext} and the results are compared for different combinations of potential strengths a , lattice angles α , cell sizes and boundary condition types. The critical value of the external magnetic field B_{cross} , at which the energy levels of the lowest two states cross, is computed for different parameters. The obtained rectangular lattice is further investigated: degeneracies between states are shown to be lifted because the system loses its rotational symmetry. Probability currents are briefly investigated, and it is shown that for weaker potentials global currents appear in a 2 by 2 cell.

Keywords

optical lattices, energy levels, avoided crossing, band structure

Title of the thesis in Polish language

Poziomy energetyczne w dwuwymiarowej zależnej od spinu sieci optycznej

Contents

1. Optical lattices	3
1.1. Introduction	3
1.2. Scalar optical lattice potential	3
1.3. Spin dependent optical lattice potential	6
1.4. Schrödinger's equation in periodic potentials.	7
2. Square lattice	8
2.1. Dirichlet boundary conditions	8
2.2. Periodic boundary conditions	13
2.3. Band structure for periodic square lattice	15
3. Rectangular lattice	18
3.1. Effect of angle between beams	18
3.2. Lattice at 85 degrees	21
3.3. Lattice at 75 degrees	23
3.4. Lattice at 60 degrees	25
3.5. Varying the shape of the lattice	27
4. 2x2 Plaquette in square and rectangular lattices	29
4.1. Square plaquette with periodic boundary conditions	29
4.2. Square plaquette with Dirichlet boundary conditions	32
4.3. Rectangular plaquette	35
4.4. Probability current	39
5. Numerical solutions	42
5.1. Finding the eigenstates with <i>Mathematica</i>	42
5.1.1. Derivation of the potential	42
5.1.2. Solving the potential using <i>NDEigensystem</i>	42
5.1.3. Analyzing the solutions	43
5.2. State tracking	44
6. Conclusions	47
6.1. Summary of results	47
6.2. Implications and future work	47

Chapter 1

Optical lattices

1.1. Introduction

Optical lattices, a powerful tool in the realm of quantum physics and condensed matter research, have garnered substantial attention for their ability to mimic complex quantum systems in a controlled laboratory environment [1]. These engineered periodic potentials are formed by interfering laser beams, where a standing electromagnetic wave can attract or repel neutral atoms into areas with stronger optical fields due to the Stark effect. Optical lattices offer a versatile platform for studying quantum phenomena, offering insights into diverse physical phenomena ranging from quantum magnetism to quantum phase transitions.

An article by P. Szulim, *et al.* 2022 [2], explores the behavior of atoms in a hexagonal 2D spin dependent optical lattice (SDOL). That work includes investigations of both single atoms, and many atoms per lattice site. The single atom Hamiltonian includes a scalar potential and a fictitious magnetic field to capture the spin interaction with the lattice. External magnetic field is applied, and phase transition is shown to occur in the many atoms limit, above some critical B_{ext} value.

This study expands upon the investigation of single bosonic atom energy levels in a SDOL, but with a rectangular symmetry. Using the Hamiltonian derived in the aforementioned work, energy eigenvalues and eigenstates are calculated numerically for different sets of parameters. A related study by I. Kuzmenko *et al.* 2023 [3] investigates fermionic atoms in a square lattice, and demonstrates the existence of a topological phase transition.

This work's main contribution is the numerical implementation of lattices with rectangular cells, achieved by changing the angle α between the 4 laser beams forming the lattice. Majority of this inquiry has the form of a systematic search over a narrow but multidimensional parameter space, where for most parameters the system behaves according to expectations. Anomalies occur in Chapter 4, where in a 2 by 2 cell avoided crossing between the states occurs, when Dirichlet boundary conditions are applied.

1.2. Scalar optical lattice potential

An optical lattice is realized using counterpropagating laser beams. In the simplest 1D case, two counterpropagating laser beams would form a standing electromagnetic wave. The atom interacts with the electric field through the Stark effect [4], and although the electric field varies over time, the average magnitude varies between the arrows and nodes of the standing wave, which results in the atom being attracted towards (or repelled from) the areas of higher electric fields (see Ref. [5]). This is known as the AC Stark effect, and it is the basis for

the periodic scalar potential that forms an optical lattice. For the derivation of the scalar potential used in this work, see the supplemental material to Ref. [2].

The resulting equation 1.1 describes the formula for the scalar potential, where α_0 is the scalar polarizability, dependent on the laser frequency ω [4].

$$V(x, y) = -\frac{\alpha_0(\omega)}{4} \mathbf{E}^*(x, y, 0) \cdot \mathbf{E}(x, y, 0) \quad (1.1)$$

To achieve a 2D optical lattice, four laser beams are required (such as on Figure 1.1a), in two counterpropagating pairs that intersect each other at an angle α (equal 90° by default), in the XY plane. In this work the beams are polarized: the \mathbf{E} vector of each beam forms a 45° angle with the XY plane, as demonstrated on Figure 1.1b. This changes the resulting scalar potential and enables a spin dependent interaction.

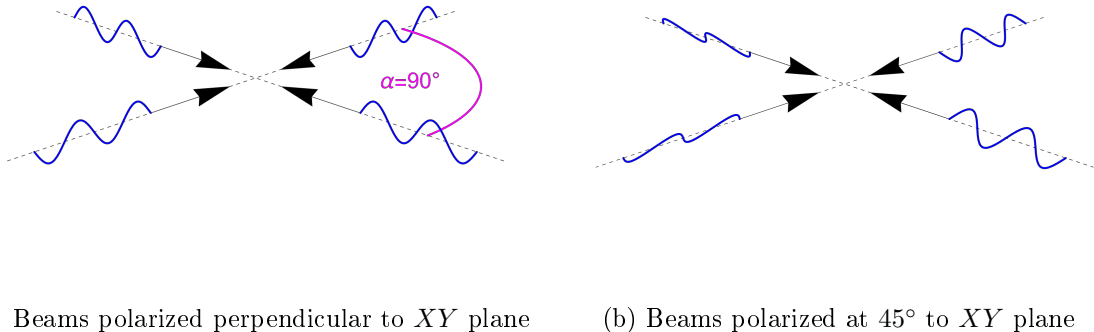


Figure 1.1: A simple schematic with four arrows symbolizing the counterpropagating beams forming a 2D optical lattice.

The interference of four linearly polarized laser beams forms a standing E_z wave, which oscillates with $e^{i\omega t}$ and Figure 1.2a shows $E_z(x, y)$ at $t = 0$. This results in a scalar potential that behaves as shown on Figure 1.2b. Because the scalar potential minima correspond to regions with the largest magnitude of electric field, the potential has a twice more frequent periodicity than E_z . This also results in the unit cell being rotated by $\alpha/2 = 45^\circ$, which in further sections is corrected for, by rotating all 4 beams for an appropriate angle.

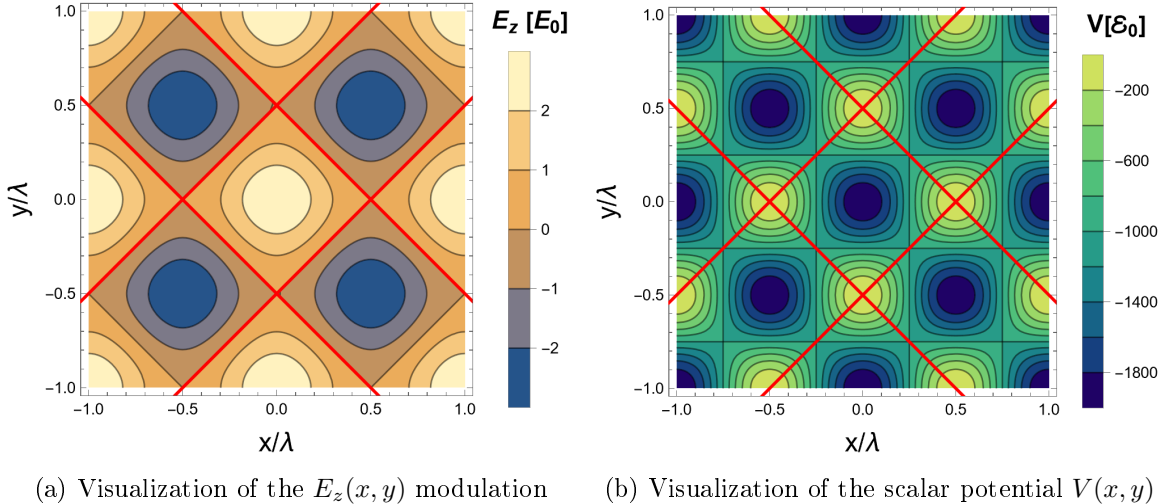


Figure 1.2: Comparison between the electric field $E_z(x, y)$ and scalar potential $V(x, y)$, with the four laser beams set along the x and y axis. The electric field is plotted at its maximum magnitude (it oscillates with $e^{i\omega t}$) in units of the amplitude of a single beam. Potential minima correspond to areas where the magnitude of E_z is highest. Because of this, the potential has a different periodicity than the electric field. In red are marked the elementary cell boundaries, which run at an $\alpha/2$ angle to the x or y axis, before the potential is rotated.

1.3. Spin dependent optical lattice potential

Apart from the scalar potential, a vector potential will be considered in this work to reflect the spin interactions with the laser beams. A fictitious magnetic field B_{fic} is used to represent the vector potential. Continuing to follow the derivations done in the supplemental material of Ref. [2], equation 1.2 shows the formula for B_{fic} . Parameter α_1 represents the vector polarizability, and I is the nuclear spin equal to 3/2.

$$g\mu_B \mathbf{B}_{\text{fic}}(x, y) = i \frac{\alpha_1(\omega)}{4(2I+1)} \mathbf{E}^*(x, y, 0) \times \mathbf{E}(x, y, 0) \quad (1.2)$$

The z component of B_{fic} is zero, and the x and y components are visualized on Figure 1.3. Similarly to hexagonal lattice in the mentioned work, the B_{fic} is lower in the center of the cell, however does not appear as isotropic.

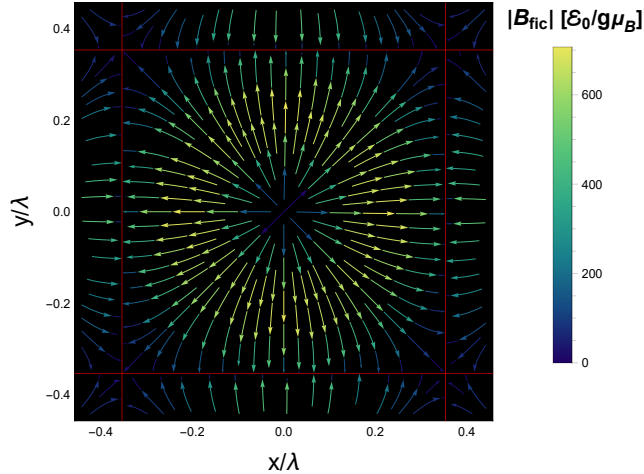


Figure 1.3: Stream plot of a fictitious magnetic field B_{fic} representing the atom's spin interaction with the electric field. The arrows indicate the direction of the field, and the color corresponds to the magnitude¹. In red are marked the boundaries between the elementary cells.

¹ Although in this work parameter a scales both the scalar and vector potential, and parameter $b = 2$ further scales B_{fic} , plots of $V(x, y)$ and B_{fic} show the values before scaling (for $a = b = 1$)

1.4. Schrödinger's equation in periodic potentials.

In the case of $\alpha = 90^\circ$, after rotating by $\alpha/2$, the scalar potential simplifies ([3]) to:

$$V(x, y) = \frac{-V_0}{2}[2 + \cos(q_0x) + \cos(q_0y)] \quad (1.3)$$

Meanwhile, the fictitious magnetic field can be written as:

$$\mathbf{B}_{\text{fic}} = -B_0\hat{\mathbf{x}}\sin(q_0x)\cos^2\left(\frac{q_0y}{2}\right) - B_0\hat{\mathbf{y}}\sin(q_0y)\cos^2\left(\frac{q_0x}{2}\right) \quad (1.4)$$

Where $q_0 = 2\sqrt{2}\pi/\lambda$. One of the most important parameters of an optical lattice is the intensity of the beam. In this work a dimensionless parameter a is used to scale both the scalar and vector potential. This means some constant laser amplitude E_0 is chosen, and is later scaled by a resulting in:

$$V_0 = a^2 \cdot \alpha_0 E_0^2 \quad (1.5)$$

Additionally, parameter b is used to scale the scalar part of the potential:

$$g\mu_B B_0 = b \cdot a^2 \cdot \alpha_1 E_0^2 \sqrt{2}/2 \quad (1.6)$$

The exact values of the parameters used in the simulations are given in Chapter 5. The distance units are scaled with the wavelength λ , while the energy is measured with $\mathcal{E}_0 = \frac{4\hbar^2\pi^4}{\lambda^2 M}$ (which is $2\pi^2$ times the recoil energy). The Hamiltonian shown on equation 1.7 incorporates both scalar and vector potential, as well as the Zeeman effect from an external magnetic field $B_{\text{ext}}\hat{\mathbf{z}}$.

$$\hat{H}(x, y) = -\frac{\hbar^2}{2M}\Delta + (V(x, y) - g\mu_B(\mathbf{B}_{\text{fic}}(x, y) + \mathbf{B}_{\text{ext}}) \cdot \mathbf{F}) \quad (1.7)$$

For Dirichlet boundary conditions, solving the potential means searching for eigenstates of the Hamiltonian. For periodic boundary conditions however, one can make use of Bloch's theorem and assume the wave function has the form: $\psi(\mathbf{r}) = e^{2\pi i \mathbf{k} \cdot \mathbf{r}/\mathbf{r}_0} \mathbf{u}(\mathbf{r})$. This allows for finding eigenstates with different values of momentum \mathbf{k} .

Chapter 2

Square lattice

The technical solutions used for solving the eigenproblem of the Hamiltonian 1.7 are described in chapter 5. Supplying the scalar and vector potential, it is possible to find energies and interpolated wave functions of n lowest eigenstates. In this work atoms of spin 1 are considered, thus the wave functions consist of three components. Two main parameters can be varied: the external magnetic field B_{ext} and the strength of the potential a . There remains the choice of either Dirichlet or periodic boundary conditions. In this chapter a 1 by 1 cell will be examined and two types of boundary conditions will be compared.

2.1. Dirichlet boundary conditions

Firstly, Dirichlet boundary conditions will be examined. An infinite potential well is constructed at the cell edges, such as is displayed on Figure 2.1a. The profile of the scalar potential along the center of the cell can be seen on Figure 2.1b.

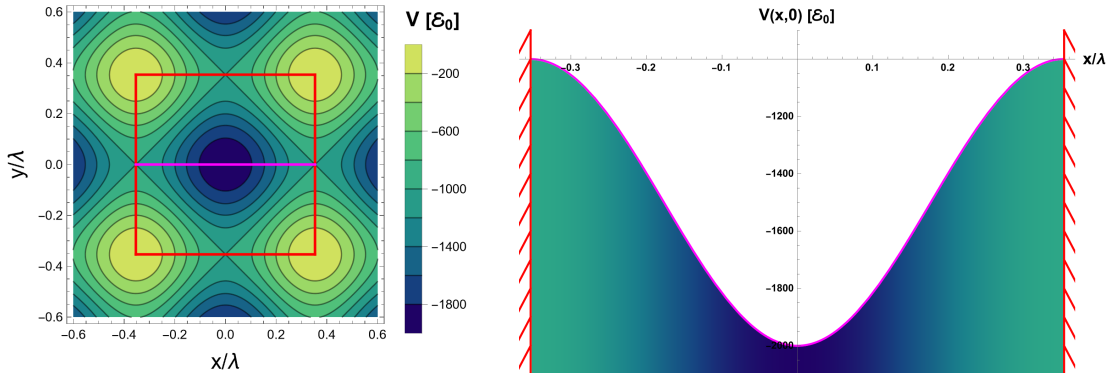


Figure 2.1: Scalar potential in the lattice with Dirichlet boundary conditions

By solving the Schrödinger equation numerically, n lowest eigenstates are obtained: their energies and interpolated wave functions. Since atoms of spin 1 are considered, the wave functions consist of three components. Two example wave functions are displayed on Figure 2.2.

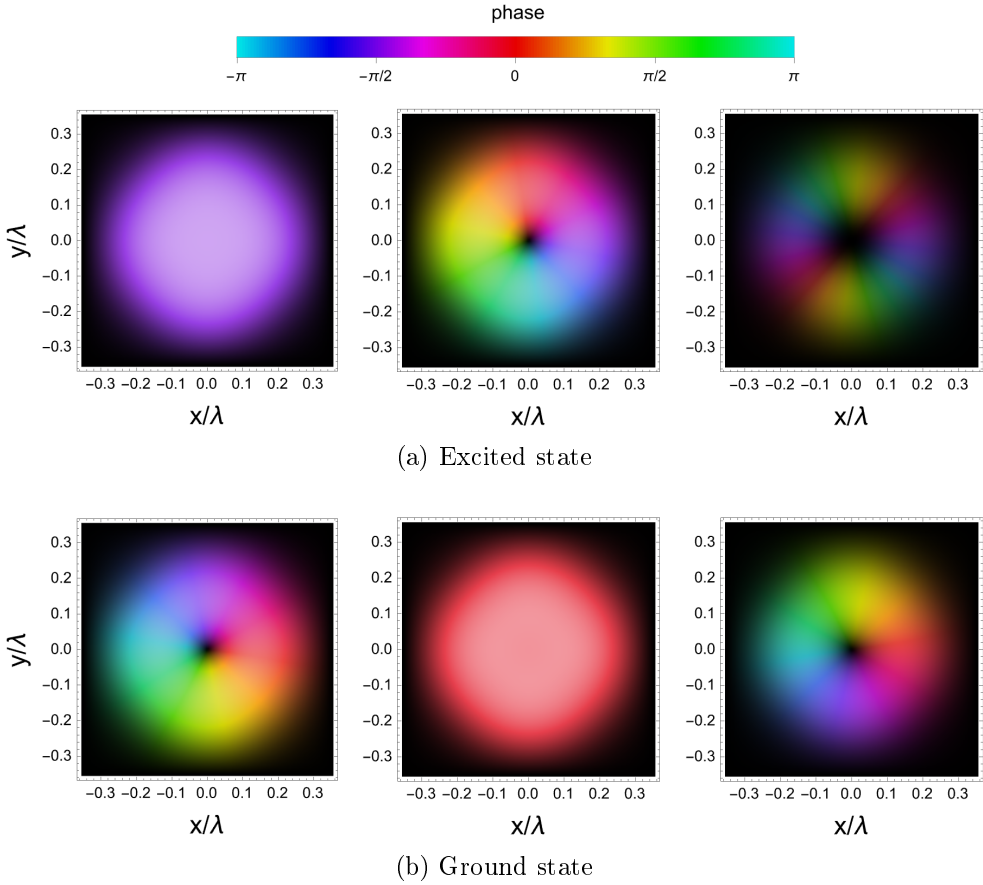


Figure 2.2: Wave functions of the ground and lowest excited state, for 1 by 1 cell with Dirichlet boundary conditions, $B_{\text{ext}} = 30 \mathcal{E}_0/(g\mu_B)$ and $a = 0.3$. The brightness of the color corresponds to the probability density (on a log scale), while hue represents the phase of the wave function. The global phase is kept as returned by the solving algorithm and can vary between states. It can be seen that the wave components form patterns, with the phase being either constant, changing clockwise or counterclockwise.

Apart from the wave functions, solving the equations for given B_{ext} gives the energies of the states. These energy levels and especially the topology of how they change with increased B_{ext} , will be the main focus of this work. Energy levels as a function of B_{ext} can be seen on Figure 2.3. In this work the states will not just be identified by their energy, but also by how they change with increased B_{ext} . Looking on the plot on Figure 2.3, three states can be identified. Let us enumerate the states in order of increasing energy at $B_{\text{ext}} = 0$. A method for tracking these states should their energies cross is needed to properly *color* the plot. This can be done either by just looking at the energies and predicting the crossing of eigenstates, but a more robust approach is to use information about the state's wave functions. Looking at Figure 2.2, which is at $B_{\text{ext}} = 30 \mathcal{E}_0/(g\mu_B)$ before the crossing, and Figure 2.4 at $B_{\text{ext}} = 40 \mathcal{E}_0/(g\mu_B)$, after the crossing, a swap within the wave functions can be noticed by looking at the first and second component of the wave function. The idea behind the algorithm used for this classification is explained on Figure 2.5, and its details are described in Chapter 5.

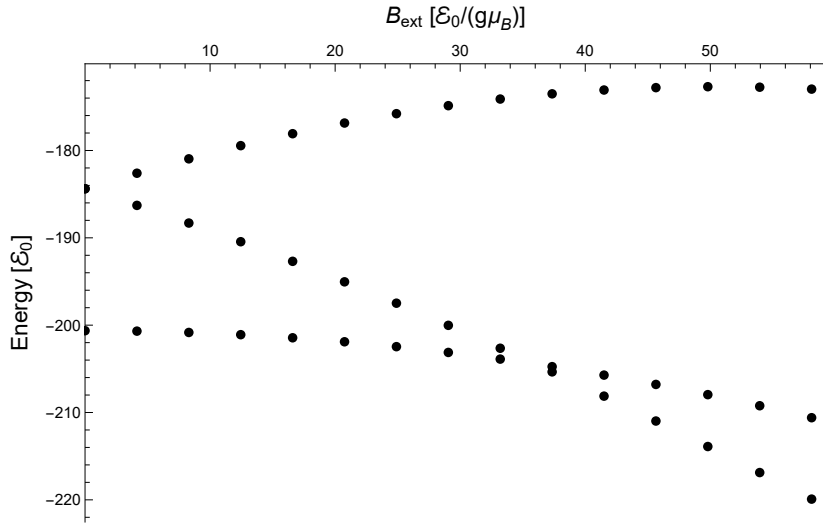


Figure 2.3: Energy levels at different values of the external magnetic field B_{ext} . Because the energies are not returned in any specific order, assigning them to specific states is non-trivial, in particular if the states appear to cross (such as states 1 and 2 at $B_{\text{ext}} \simeq 36 \mathcal{E}_0/(g\mu_B)$.)

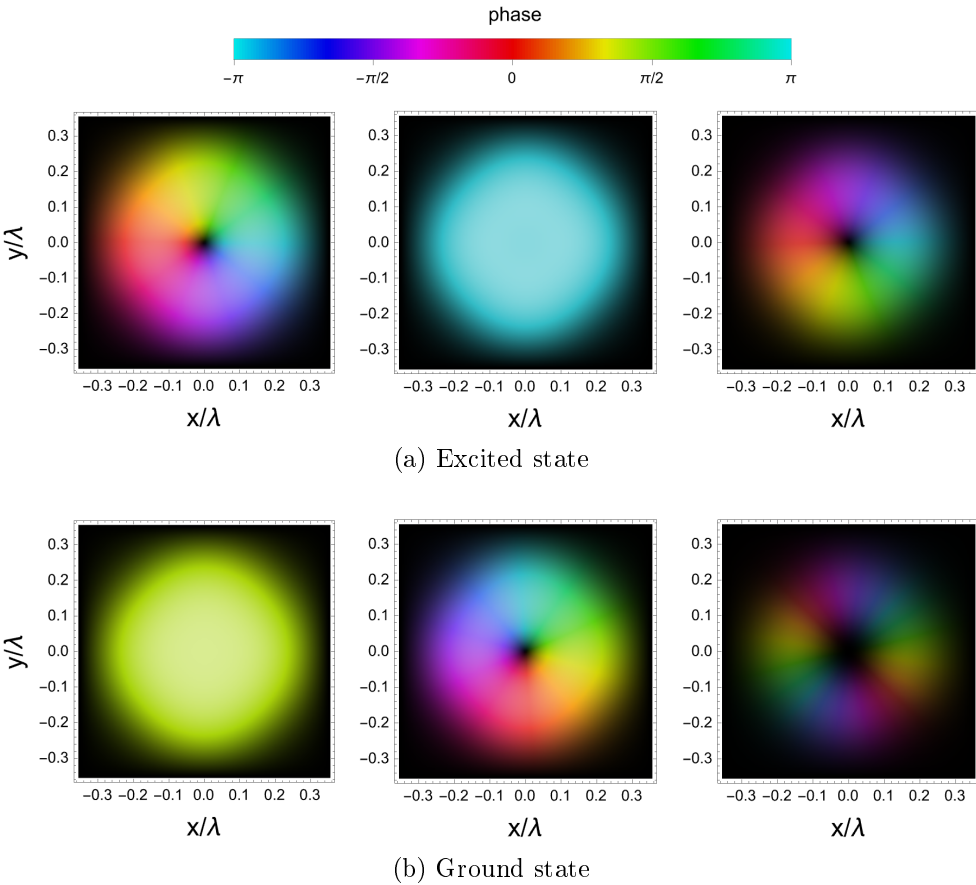


Figure 2.4: Wave functions of the ground and first excited state, for a 1 by 1 cell with Dirichlet boundary conditions, $B_{\text{ext}} = 40 \mathcal{E}_0/(g\mu_B)$ and $a = 0.3$. By comparison to Figure 2.2, it is apparent the states have swapped places.

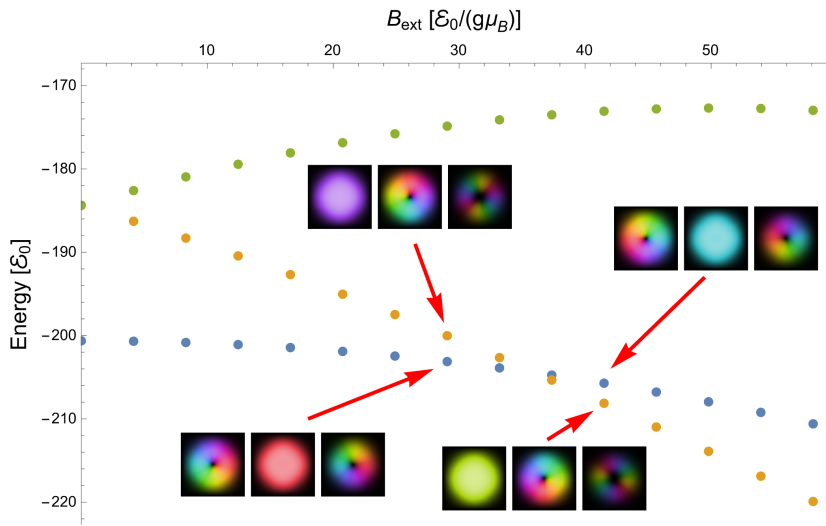


Figure 2.5: Energies of the lowest three eigenstates in 1 by 1 cell with Dirichlet boundary conditions, for $a = 0.3$ and different B_{ext} . On the plot the method used for detecting crossings is highlighted. The final resulting plot can be seen on Figure 2.6.

With the ability to classify correlated eigenstates, it is possible to draw plots such as on Figure 2.6. The external magnetic field B_{cross} , defined as B_{ext} at which the ground state has the same energy as the excited state, can give information about the scale at which the external magnetic field impacts the topology of the energy levels. In example, at Figure 2.7, the depth of the potential is scaled with $a = 0.15$ squared, resulting in a 4 times shallower potential than that on Figure 2.6. This result in the B_{cross} value being significantly smaller. The exact correlation of B_{cross} as a function of a seems to be quadratic, as displayed on Figure 2.9. An extension of the plot at Figure 2.6 can be seen on Figure 4.9b, showing the evolution of the lowest 9 states.

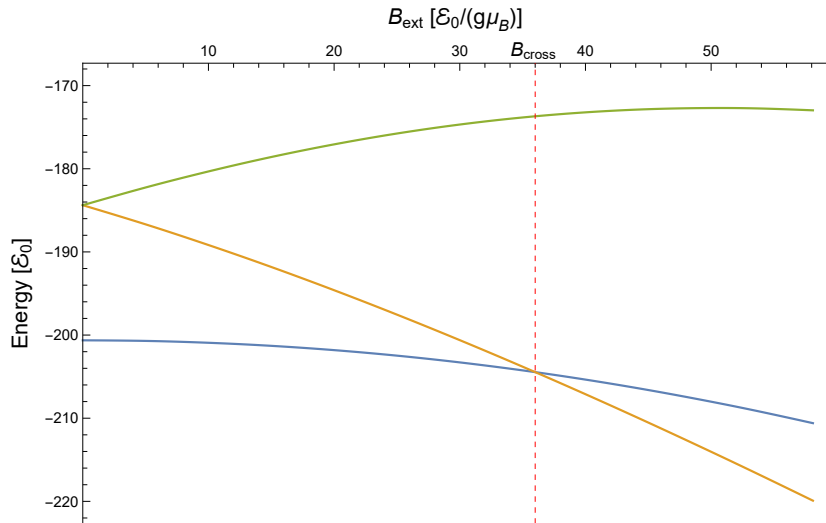


Figure 2.6: Plot of energy levels as a function of B_{ext} , for $a = 0.3$ in a 1 by 1 cell with Dirichlet boundary conditions. States two and three are degenerate at $B_{\text{ext}} = 0$, and the ground state crosses with the excited state at $B_{\text{cross}} \simeq 36 E_0/(g\mu_B)$.

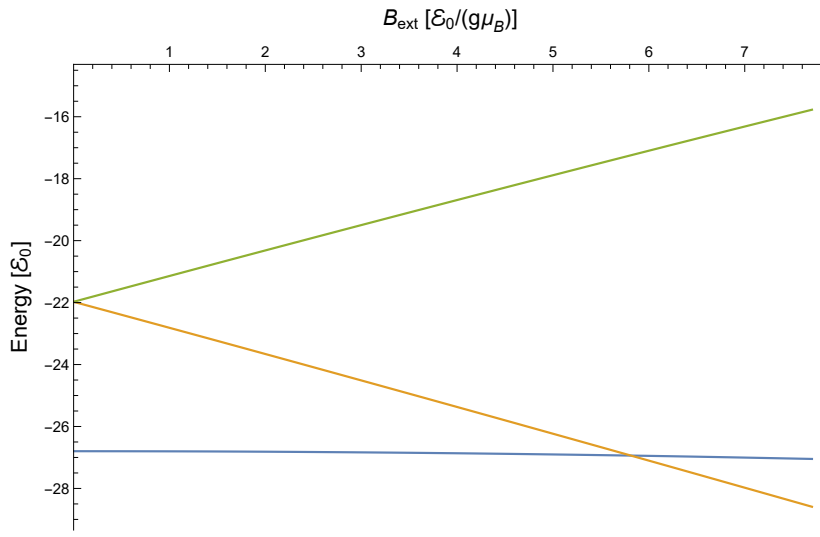


Figure 2.7: Plot of energy levels as a function of B_{ext} , for $a = 0.15$ in a 1 by 1 cell with Dirichlet boundary conditions. Compared to Figure 2.6, the energies change more linearly with B_{ext} and B_{cross} is smaller at around $5.5 \mathcal{E}_0/(g\mu_B)$.

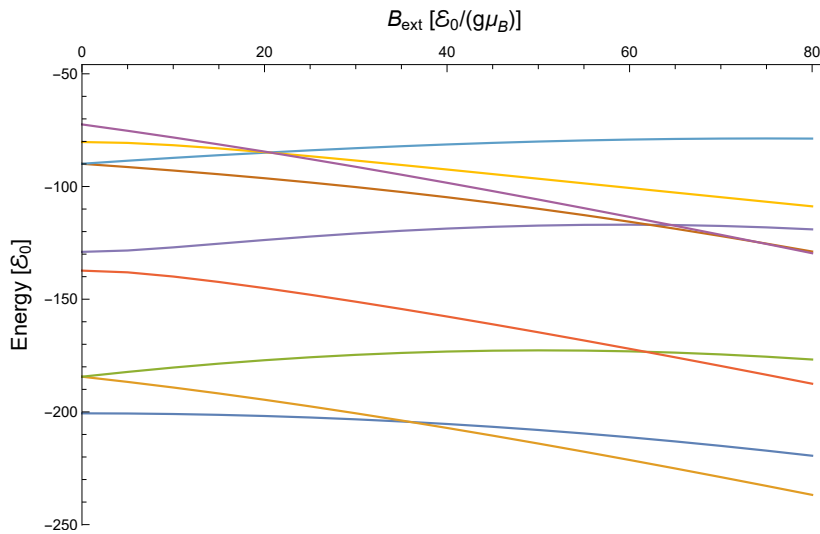


Figure 2.8: Extension of the plot at Figure 2.6: nine lowest energy levels as a function of B_{ext} , for $a = 0.3$ in a 1 by 1 cell with Dirichlet boundary conditions. Similar to states 2 and 3, states 6 and 7 are degenerate at $B_{\text{ext}} = 0$. Notice states 7, 8 and 9 crossing at $B_{\text{ext}} \simeq 20 \mathcal{E}_0/(g\mu_B)$.

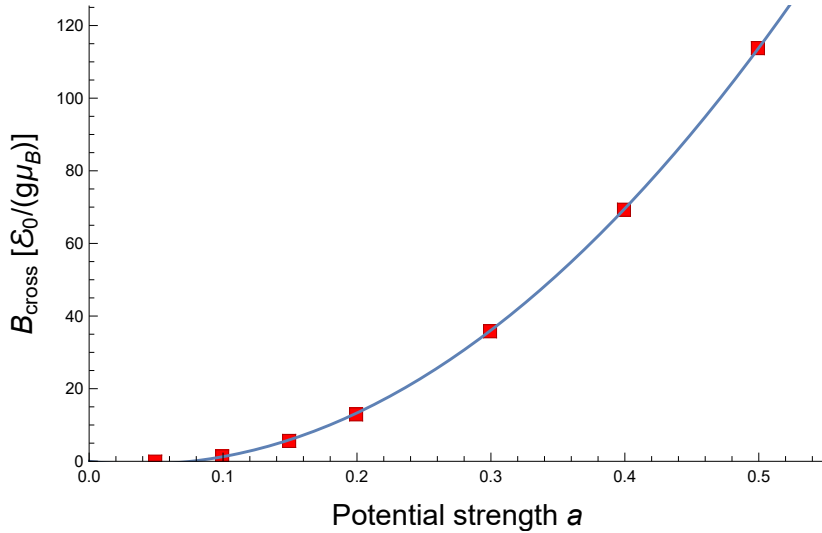
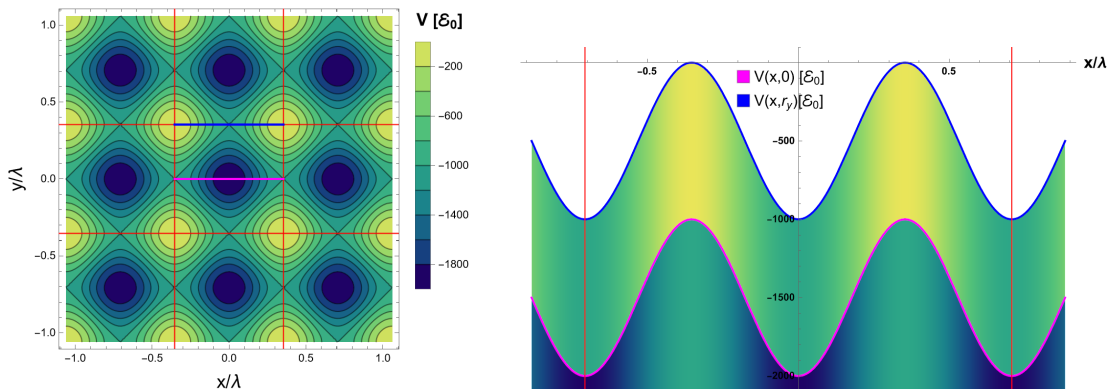


Figure 2.9: Estimated crossing of the ground and excited state B_{cross} as a function of the parameter a , which scales the depth of the potential. Calculated for a 1 by 1 cell with Dirichlet boundary conditions. Fitted is a parabola $B_{\text{cross}} = (540a - 40)\mathcal{E}_0/(g\mu_B)$

2.2. Periodic boundary conditions

As mentioned before, periodic boundary conditions can be imposed when searching for eigenstates. The periodic conditions are imposed on the cell boundaries, as shown of Figure 2.10a. In the Dirichlet boundary conditions, there exists a hard wall between cells. In periodic boundary conditions, between two cells exists a saddle point in the scalar potential. The cross-section of the potential in the center and the boundary of the cell can be seen on Figure 2.10b.



(a) Scalar potential as a function of x and y . In red are marked the edges of the elementary cells, along which periodic boundary conditions are applied.

(b) Scalar potential at $y = 0$ (magenta) and $y = r_y$ (blue). The potential at $y = r_y$ is shifted by a constant amount.

Figure 2.10: Scalar potential in the lattice with periodic boundary conditions

The difference in solutions between different boundary conditions will be a focus of interest in this work. One should expect the solutions to look similar for lower states, as then the function is localized away from the boundaries of the cell. For eigenstates with higher energies,

it is likely for the solutions to differ, especially because of interactions between cells. The wave functions of three lowest eigenstates for $B_{\text{ext}} = 30 \mathcal{E}_0/(g\mu_B)$ are displayed on Figure 2.11 and the two lowest states are similar to those on Figure 2.2 (Dirichlet BC), with accuracy to global phase. The lower energy levels behave very similarly with varying B_{ext} , as can be seen by comparing Figures 2.12a and 2.12b to 2.6 and 2.7. There is however a slight difference in the behavior of the higher eigenstates, noticeable by comparing Figure 2.12c to Figure 2.8. States 7, 8 and 9 appear to cross with Dirichlet boundary conditions, but avoid crossing with periodic boundary conditions.

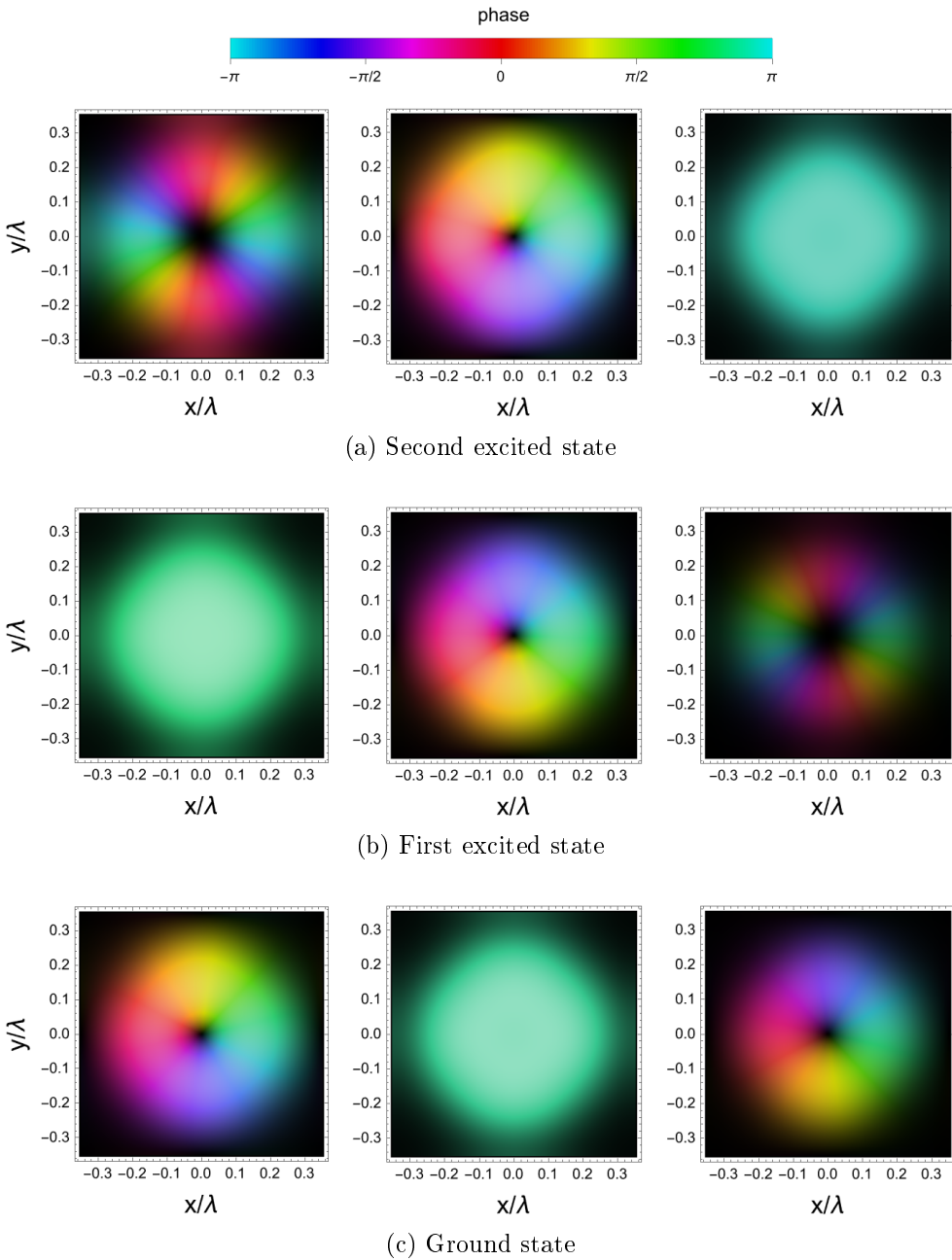


Figure 2.11: Wave functions of the ground and two excited states, for 1 by 1 cell with periodic boundary conditions, $B_{\text{ext}} = 30 \mathcal{E}_0/(g\mu_B)$ and $a = 0.3$.

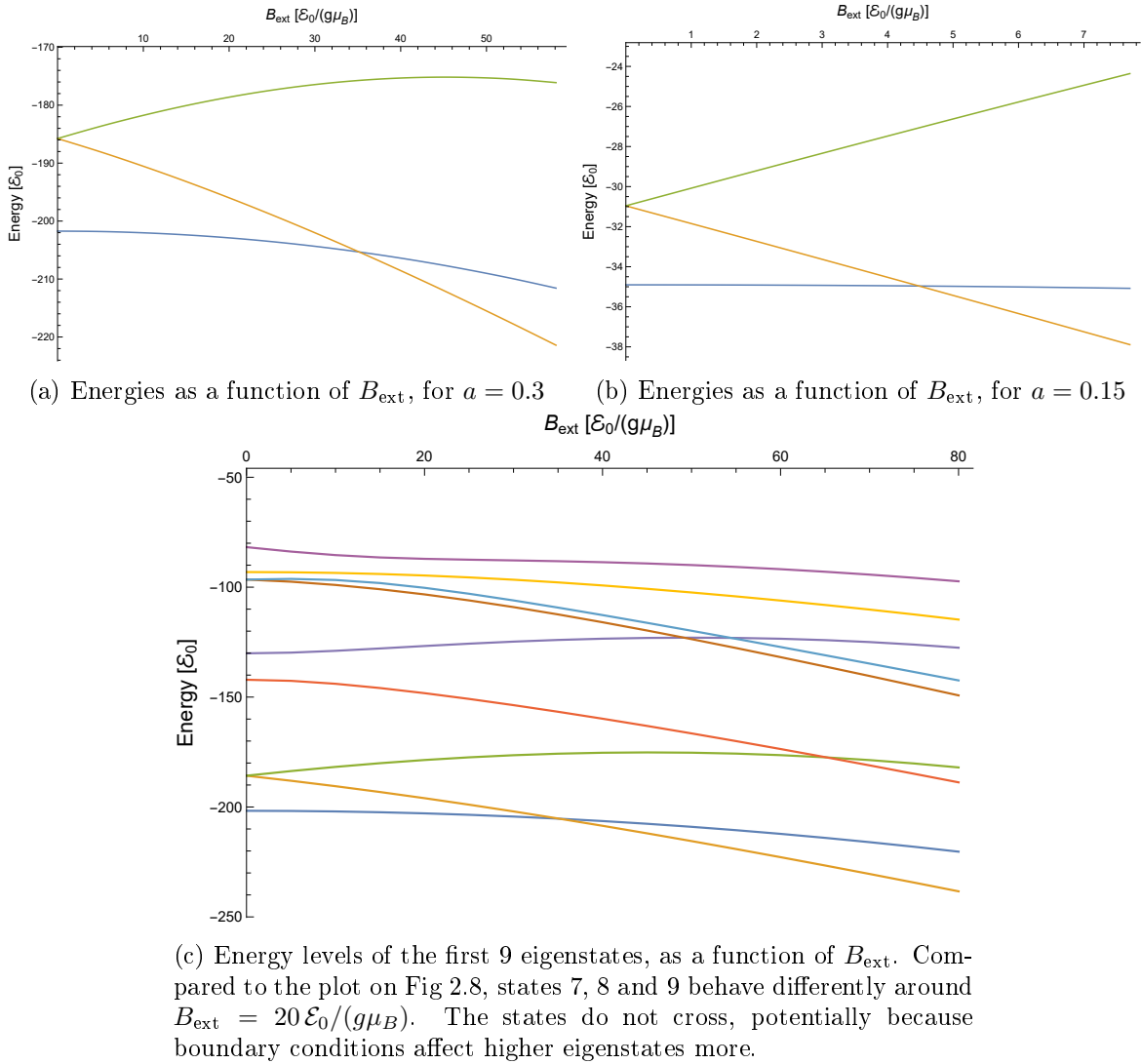


Figure 2.12: Energy levels as a function of B_{ext} in a 1 by 1 cell with periodic boundary conditions.

2.3. Band structure for periodic square lattice

In the case of the periodic boundary conditions, making use of Bloch's theorem, the solution is assumed to be of the form $\psi(\mathbf{r}) = e^{2\pi i \mathbf{k} \cdot \mathbf{r}/r_0} \mathbf{u}(\mathbf{r})$ (where r_0 would be the lattice periodicity). The x and y momentum: k_x and k_y can be chosen prior to solving the Schrödinger equation. In this work $k_x = k_y = 0$ is generally used, but nonzero momentum can be implemented, and Figure 2.13 shows the wave functions resulting from $k_x = 0.5q_0$, where $q_0 = 2\pi/\lambda$.

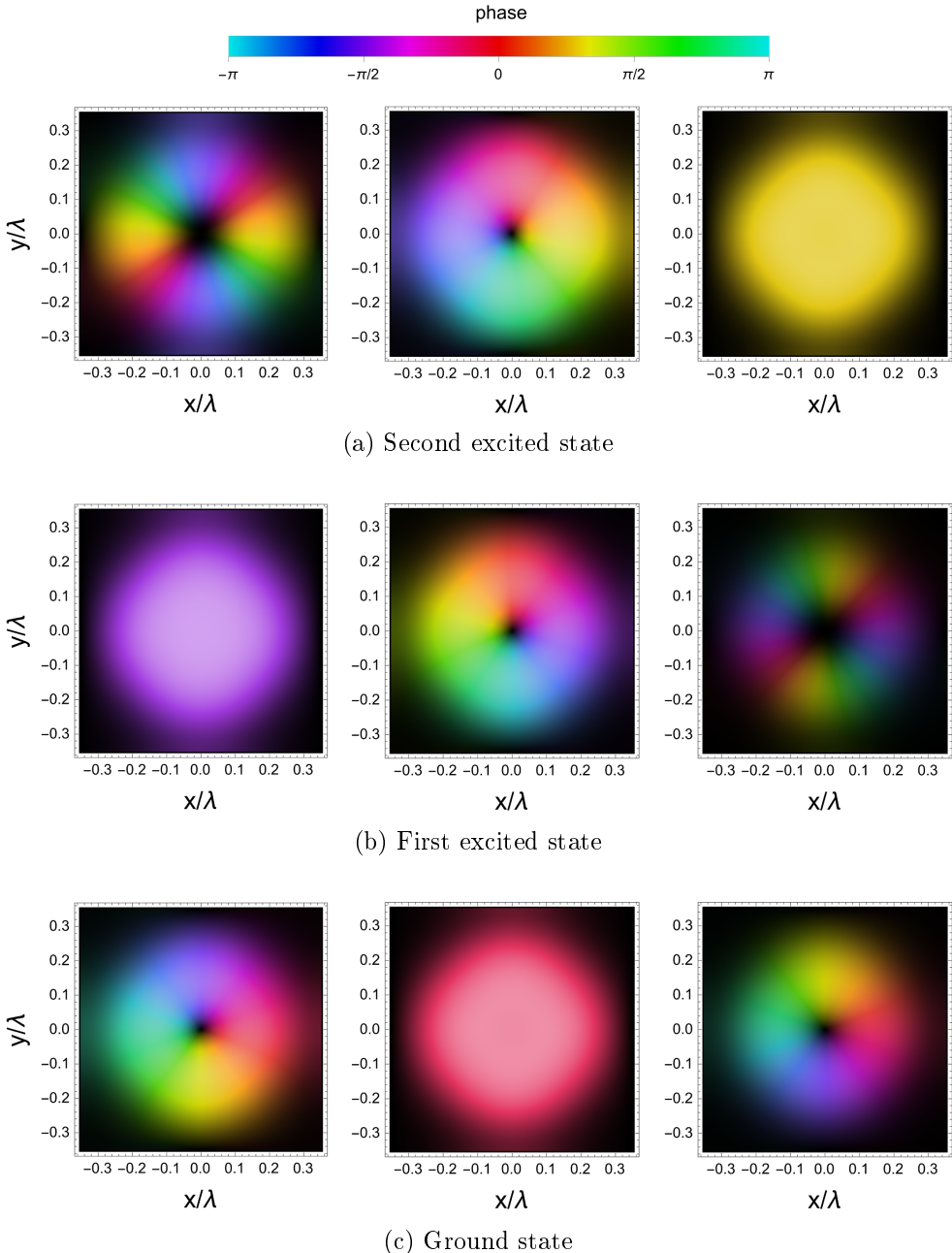


Figure 2.13: Wave functions of the ground and two excited states, for 1 by 1 cell with periodic boundary conditions, $B_{\text{ext}} = 3\mathcal{E}_0/(g\mu_B)$, $a = 0.3$ and $k_x = 0.5q_0$. As can be seen above, introducing $k_x \neq 0$ does not change the characteristic of the solution.

Neither the wave functions, nor the energy of the eigenstates changes significantly with the increase of k . The effect is even less noticeable for stronger potentials. The band resulting band structure for $a = 0.3$ and $B_{\text{ext}} = B_{\text{cross}}$ can be seen on Figure 2.14. Because of symmetry, at $\alpha = 90^\circ$ changing k_x has the same effect as changing k_y . On Figure 2.15 multiple energy from B_{ext} plots are superimposed, for k_y ranging from 0 to $0.5q_0$.

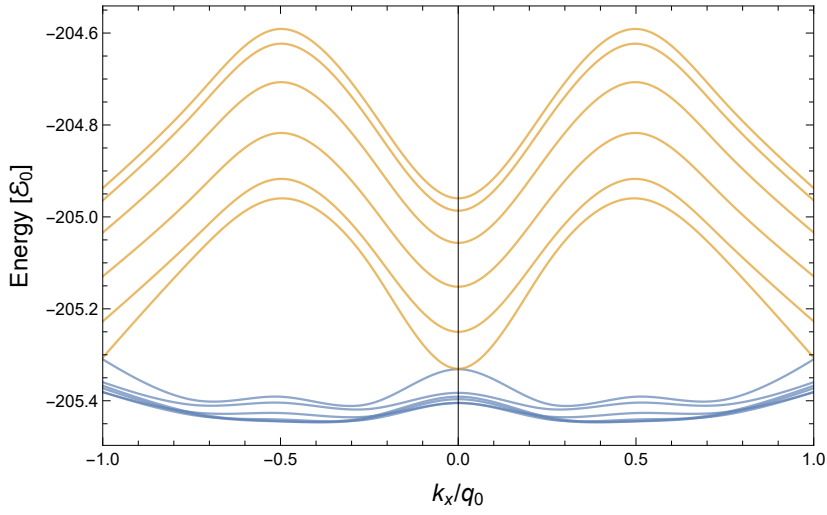


Figure 2.14: Band structure of the ground and excited state, for $a = 0.3$ and $B_{\text{ext}} = B_{\text{cross}} \simeq 36 E_0/(g\mu_B)$. The horizontal axis represents the change in k_x and the multiple lines are generated with different values of k_y . The energy varies only slightly, because of the strength of the potential.

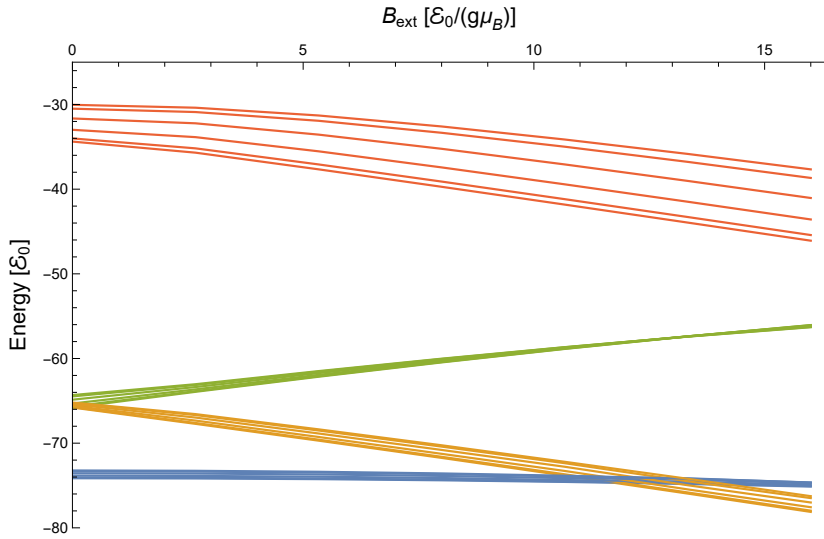


Figure 2.15: Plot of energy levels as a function of B_{ext} , for $a = 0.2$ and k_y between 0 and $0.5 q_0$. The difference in energy is largest in the fourth state.

Chapter 3

Rectangular lattice

3.1. Effect of angle between beams

The potential of the lattice is derived from two pairs of counterpropagating beams of light. In the previous chapter, the angle α between those two pairs was set to 90° . This resulted in 90° rotational symmetry of the potential. By changing the angle between the beams the dimensions of the elementary cell change, resulting in a rectangular, rather than square grid. The effect of reducing the angle to 60° is displayed on Figure 3.1.

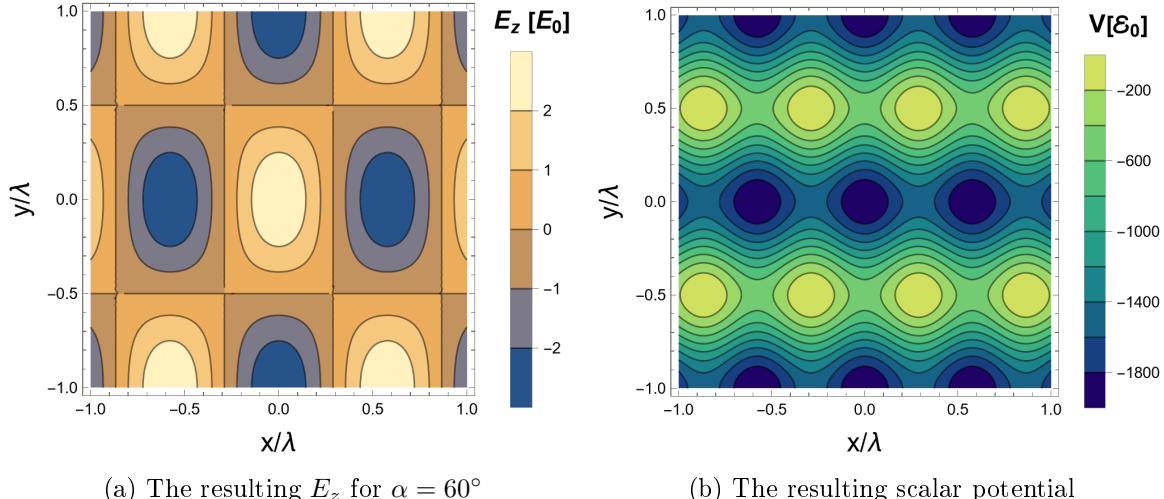


Figure 3.1: The E_z and scalar potential in the lattice. The angle between beams is set to 60° . The E_z is shown at maximum magnitude, in units of the amplitude of a single laser beam. Because the Stark effect is related to the magnitude of the electrical field, the periodicity of the potential is different from that of the E_z . Highest magnitudes of E_z correspond to potential minima and lowest magnitudes to maxima. Apart from the change in the dimensions of the elementary cell, worth noting is the difference in potential between the saddle points at x and y boundaries of the cell.

On Figure 3.2, the boundaries of an elementary cell are marked on the scalar potential. The cell is a rectangle with height $2r_y$ and width $2r_x$, where the formula for obtaining the size of the cell is:

$$\begin{aligned} r_x &= \lambda/(4 \cos(\alpha/2)) \\ r_y &= \lambda/(4 \sin(\alpha/2)) \end{aligned} \tag{3.1}$$

The details of implementing the rectangular lattice are described in further detail in Chapter 5. When $\alpha = 90^\circ$, the elementary cell becomes a square with a side of $\lambda/2\sqrt{2}$. As α goes below 60° the scalar potential at the saddle point on the $x = \pm r_x$ becomes lower, which makes the interaction between cells stronger along the x direction. This also makes the Dirichlet boundary conditions more invasive, while periodic boundary conditions raise concerns about the precision of the solution. For this reason angles above 45° will be considered. It is worth noting that as α approaches 0° , the lattice becomes one dimensional, but counterintuitively, along the x axis (since r_y goes to infinity). A comparison between cell dimensions and scalar potentials for different angles α can be seen on Figure 3.3.

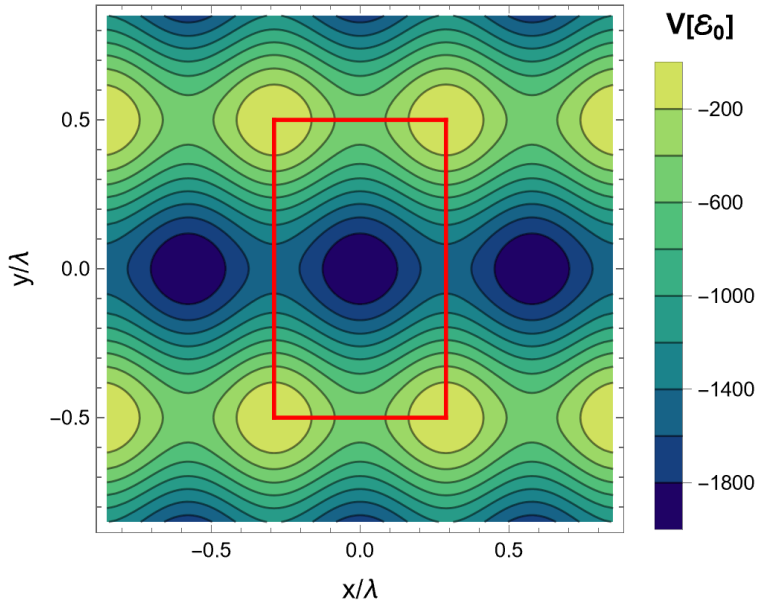


Figure 3.2: Elementary cell on the scalar potential for $\alpha = 60^\circ$. The cell is a rectangle with sides $1/\sqrt{3}$ and 1.

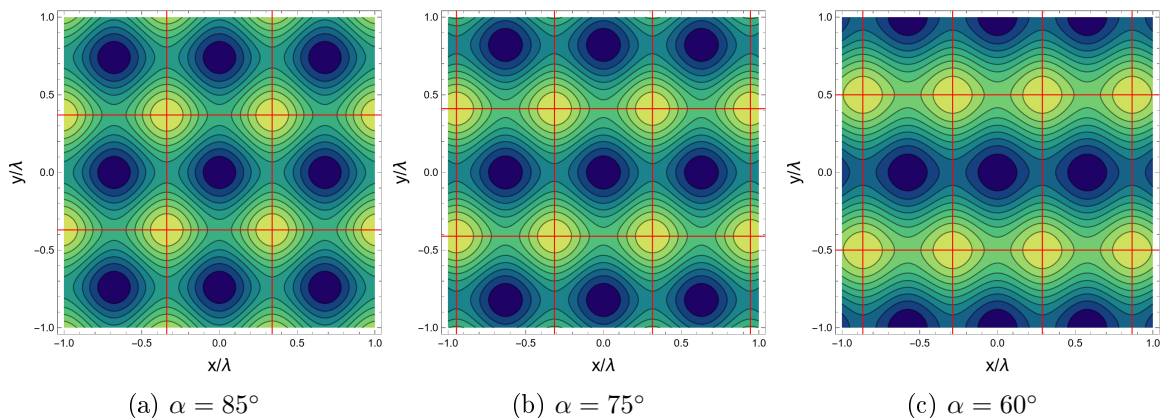


Figure 3.3: Scalar potentials for different angles α . In red are highlighted the boundaries between cells.

Worth investigating are the changes, that lowering the angle α induces on the fictitious magnetic field B_{fic} . Figure 3.4 shows stream plots of B_{fic} for $\alpha = 85^\circ$ and $\alpha = 75^\circ$. The scalar potential changes to match the size of the cell, and reaches larger magnitudes along the

x axis. Figure 3.5 shows a similar stream plot alongside a cross-section through the x and y axis. Interestingly, the potential is anisotropic also near the very center of the cell (Fig. 3.5b), as opposed to the scalar potential (Figures 3.6b, 3.10b and 3.14b). This effect is also present for angles 75° and 85°. This is an important discovery, because it suggests that even states located far from the cell's boundaries will experience the asymmetry between the x and y direction.

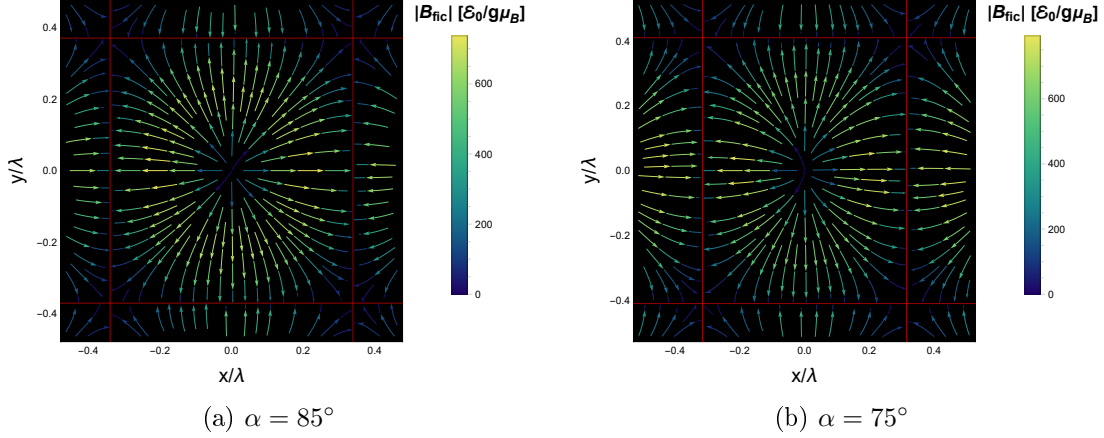


Figure 3.4: Vector potential, in form of a fictitious magnetic field B_{fic} for different angles α . In red are highlighted the boundaries between cells.

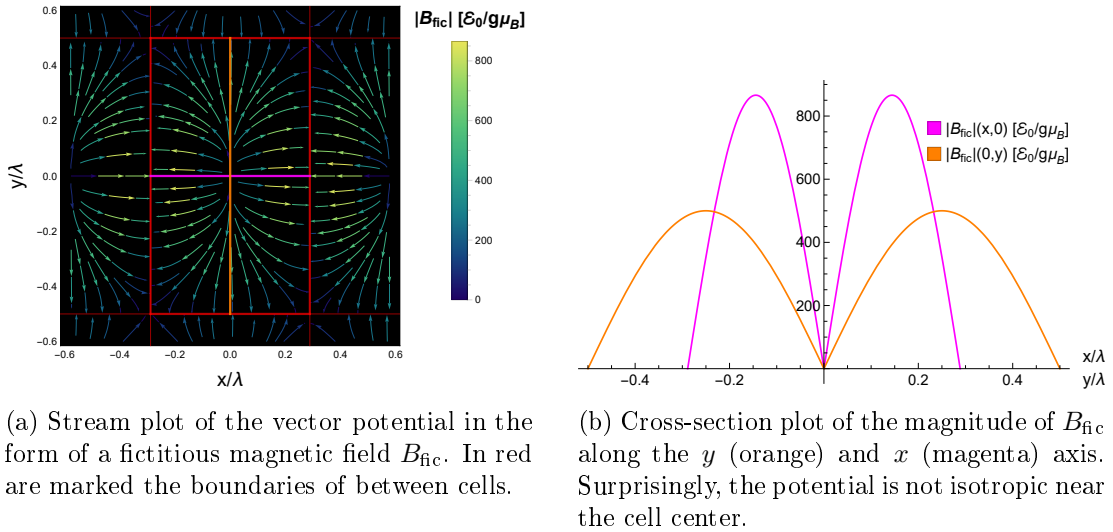
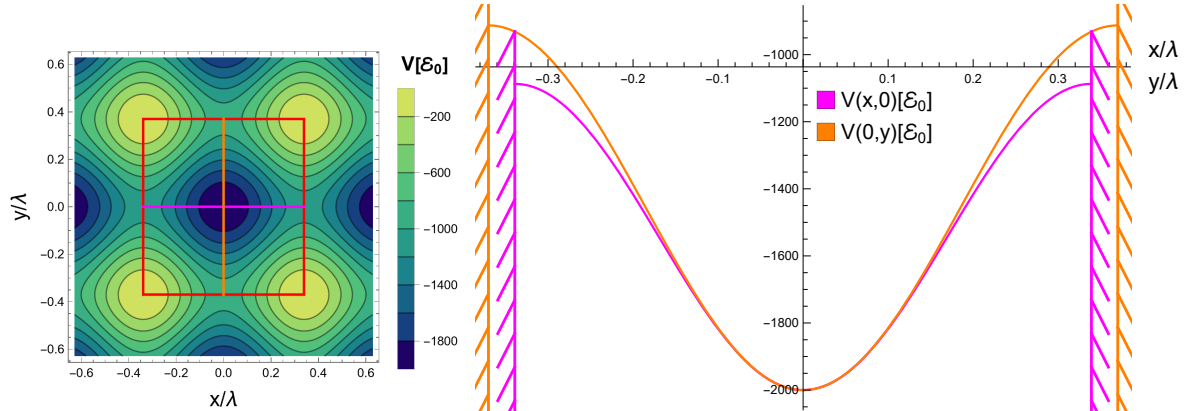


Figure 3.5: Fictitious magnetic field B_{fic} for $\alpha = 60^\circ$.

In the further part of this chapter, the angle α will be gradually reduced, and the results compared to those obtained for $\alpha = 90^\circ$.

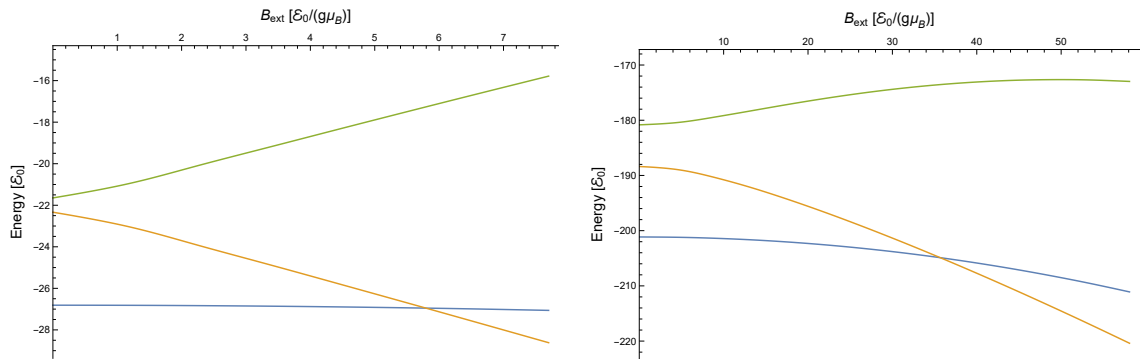
3.2. Lattice at 85 degrees

With the angle reduced only slightly to $\alpha = 85^\circ$, the potential remains similar, as shown on Figure 3.6. On Figure 3.7 energy levels plotted, and the resulting plots look similar to those on Figure 2.6 and Figure 2.7, except for the lifted degeneracy between first and second excited states, at $B_{\text{ext}} = 0$. On Figure 3.8 the wave functions of first two states at $B_{\text{ext}} = 25 \mathcal{E}_0/(g\mu_B)$ are displayed. A comparison of the energy levels of the first 9 states, between Dirichlet and periodic boundary conditions is displayed on Figure 3.9.



(a) Scalar potential with the elementary cell marked in red. The potential and $x = 0$ (orange). Marked are also the Dirichlet boundary conditions, at different distances from the cell's center in both directions. Interestingly, although the length of the cell's sides and the potential maximum value differs between directions, the shape of the potential near the center of the cell is the same, which means there the potential is isotropic.

Figure 3.6: Scalar potential for $\alpha = 85^\circ$



(a) Energies as a function of B_{ext} , for $a = 0.15$. The degeneracy between states two and three at $B_{\text{ext}} = 0$ is lifted, as opposed to the plot on Figure 2.7.

(b) Energies as a function of B_{ext} , for $a = 0.3$. The gap between the energies of states 2 and 3 at $B_{\text{ext}} = 0$ is more significant than that on Figure 3.7a.

Figure 3.7: Energy levels as a function of B_{ext} in a 1 by 1 cell with Dirichlet boundary conditions, for $\alpha = 85^\circ$.

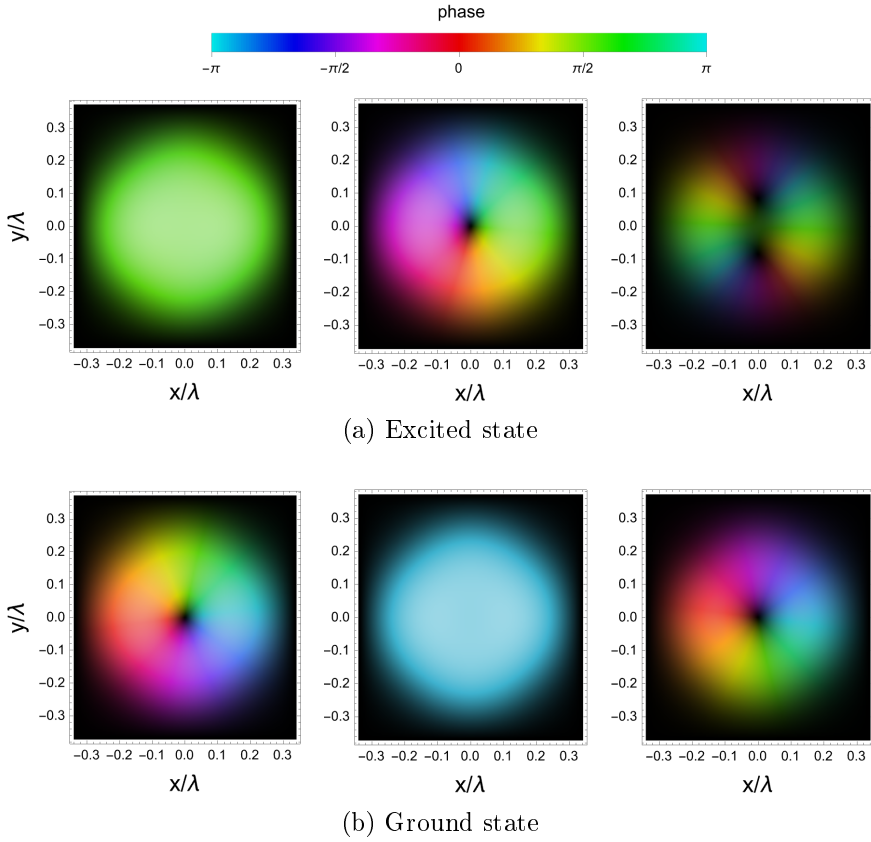


Figure 3.8: Wave functions of the ground and excited state, for 1 by 1 cell with Dirichlet boundary conditions, $\alpha = 85^\circ$, $B_{\text{ext}} = 25 \mathcal{E}_0/(g\mu_B)$ and $a = 0.3$. The resulting wave functions are similar to those on Figure 2.2, but are elongated to match the different dimensions of the cell.

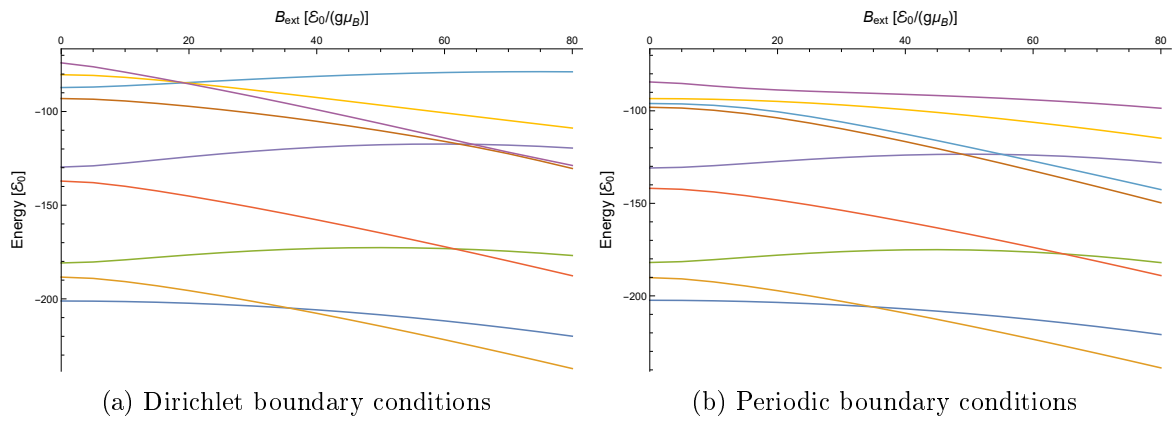
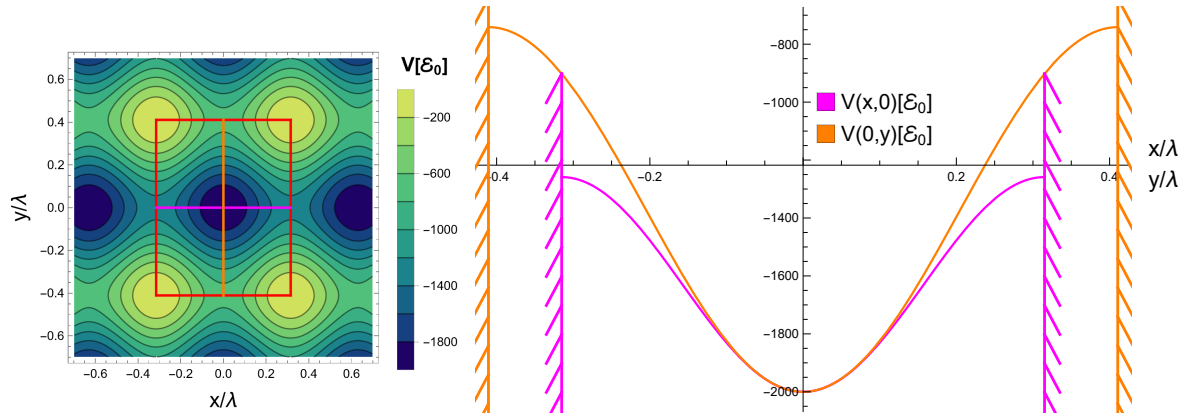


Figure 3.9: Energy levels of the first 9 eigenstates, as a function of B_{ext} , for $\alpha = 85^\circ$. The plots look alike to those on Figures 2.8 and 2.12c, and show similar behavior between states 7, 8 and 9 for Dirichlet and periodic boundary conditions.

3.3. Lattice at 75 degrees

At $\alpha = 75^\circ$ the potential still resembles the structure of a 2D lattice, while having significant changes to the proportions of the cell sides. This perhaps makes it the angle most suitable to draw conclusions from about the behavior of the eigenstates at angles less than 90° .

As can be seen on Figure 3.10, the scalar potential has noticeable differences compared to the case of $\alpha = 90^\circ$. Energy levels as a function of B_{ext} are plotted on Figure 3.11. The gap between the energies of states 2 and 3 at $B_{\text{ext}} = 0$ is larger than on the corresponding plots on Figure 3.7. The wave functions displayed in Figure 3.12 are more stretched, but other than that, they are similar to those shown before. The energy levels of the first 9 states, both with Dirichlet and periodic boundary conditions are displayed on Figure 3.13.



(a) Scalar potential with the elementary cell marked in red. The shape of the $x = 0$ (orange). While the potential behaves differently near the boundaries, it is isotropic near the cell's center.
(b) Scalar potential cross-section along $y = 0$ (magenta) and $x = 0$ (orange). The shape of the $x = 0$ (orange). While the potential behaves differently near the boundaries, it is isotropic near the cell's center.
(c) Scalar potential with the elementary cell marked in red. The shape of the $x = 0$ (orange). While the potential behaves differently near the boundaries, it is isotropic near the cell's center.

Figure 3.10: Scalar potential for $\alpha = 75^\circ$

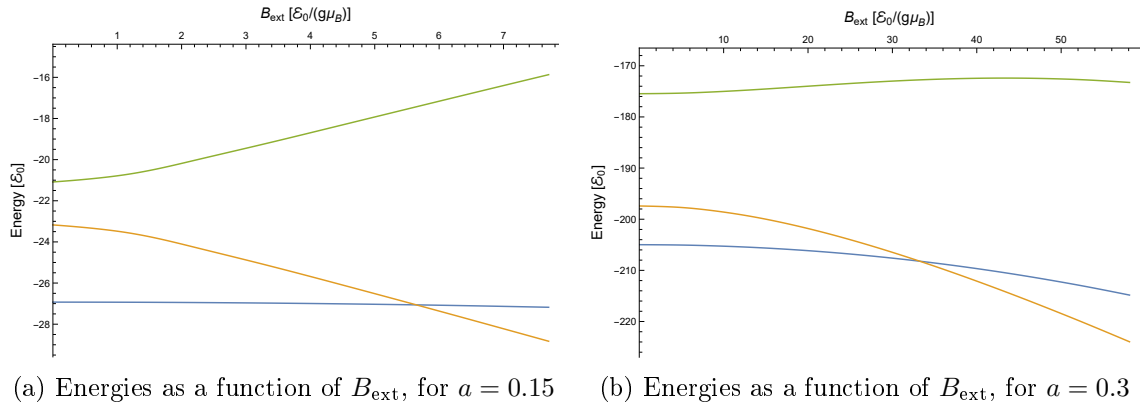


Figure 3.11: Energy levels as a function of B_{ext} in a 1 by 1 cell with Dirichlet boundary conditions, for $\alpha = 75^\circ$. Compared to plots on Figure 3.7, the gap between state 2 and 3 is larger.

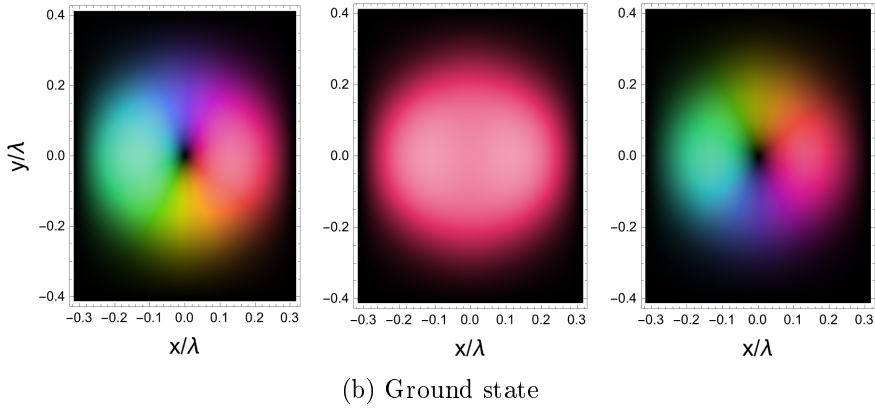
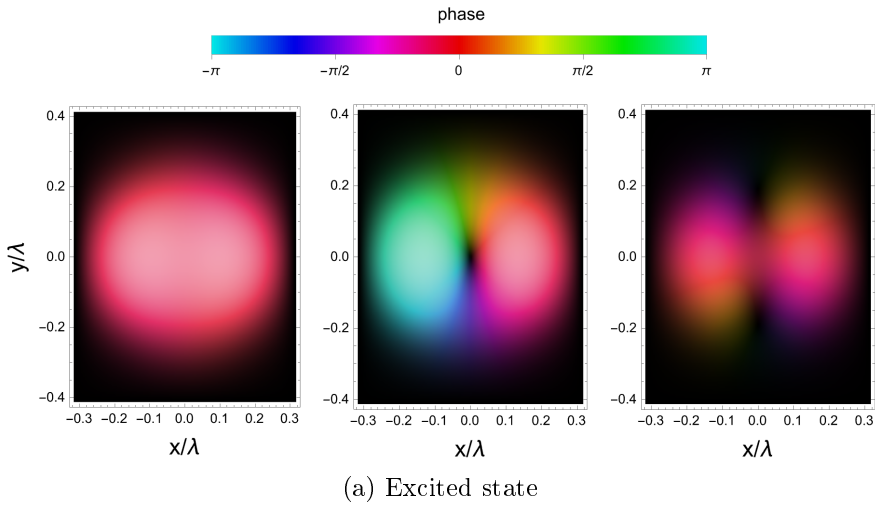


Figure 3.12: Wave functions of the ground and excited state, for 1 by 1 cell with Dirichlet boundary conditions, $\alpha = 75^\circ$, $B_{\text{ext}} = 25 \mathcal{E}_0/(g\mu_B)$ and $a = 0.3$.

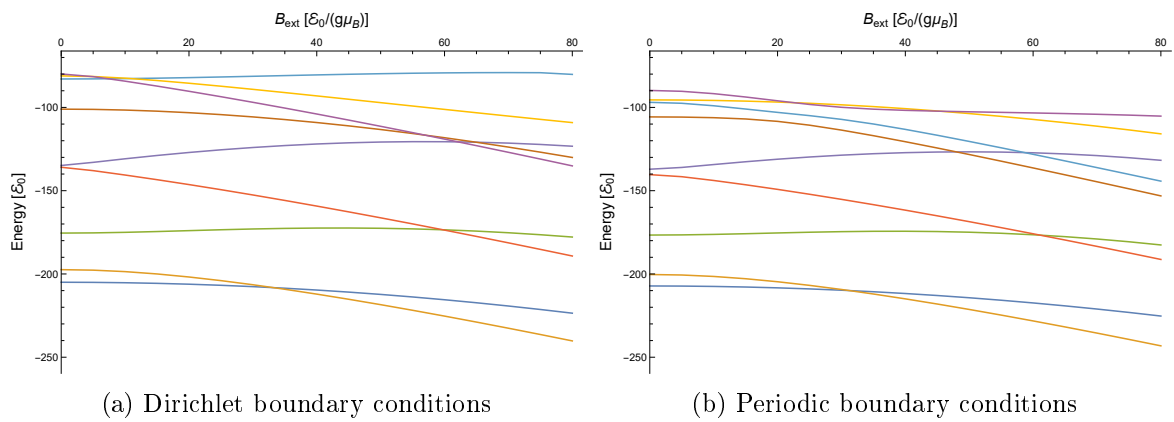


Figure 3.13: Energy levels of the first 9 eigenstates, as a function of B_{ext} , for $\alpha = 75^\circ$. Some difference between boundary condition type can still be observed.

3.4. Lattice at 60 degrees

At $\alpha = 60^\circ$ the potential starts to look very different, resembling more a 1 dimensional lattice in the y direction. As displayed on Figure 3.14a, the cells dimensions differ by a factor of almost 2 and Figure 3.14b shows how shallow the potential is in the x direction.

Energies of the eigenstates as a function of B_{ext} are plotted on Figure 3.15. The wave functions at $B_{\text{ext}} = 25 \mathcal{E}_0/(g\mu_B)$ displayed on Figure 3.16 continue the trend of vertical elongation, however without noticeable topological differences. Plots on Figure 3.17 showing the energies of the first 9 eigenstates, also do not differ much from the results for α equal 85° and 75° .

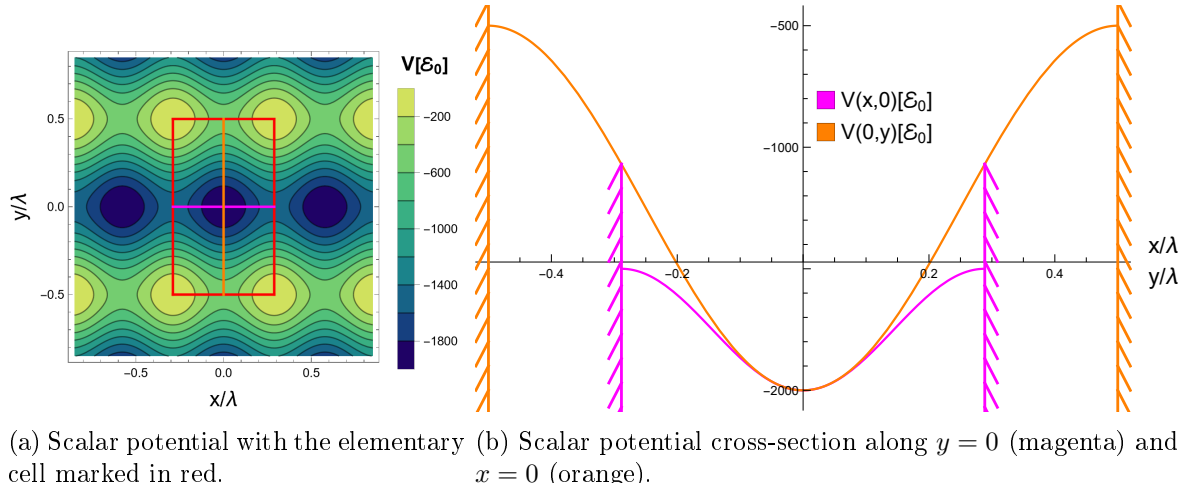


Figure 3.14: Scalar potential for $\alpha = 60^\circ$

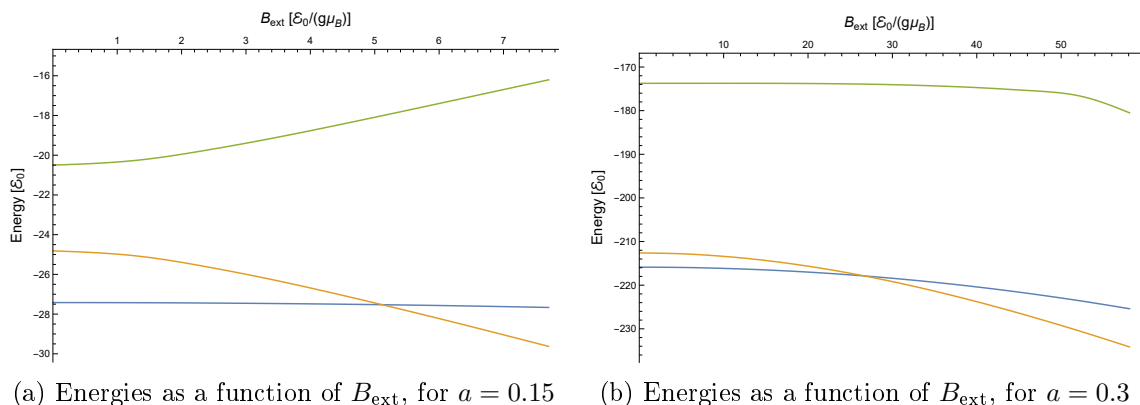
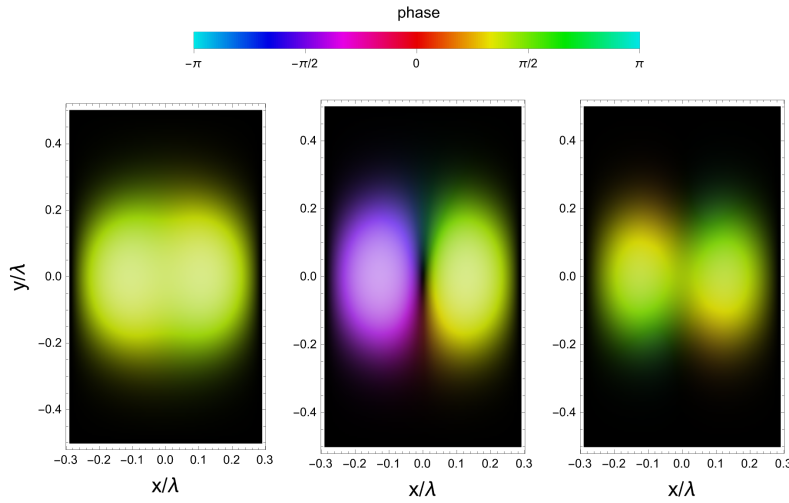
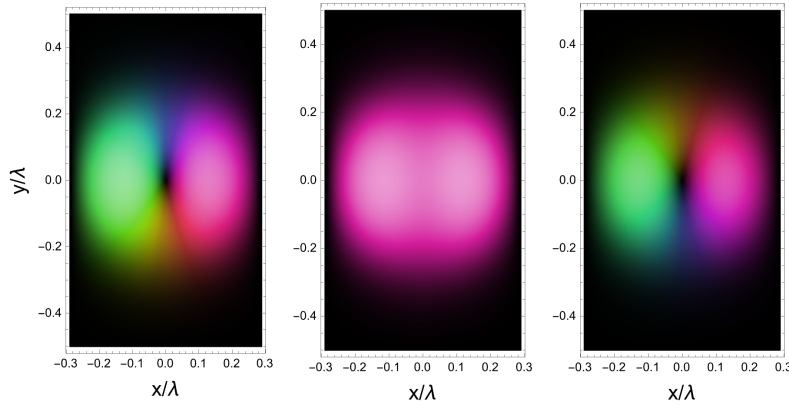


Figure 3.15: Energy levels as a function of B_{ext} in a 1 by 1 cell with Dirichlet boundary conditions, for $\alpha = 60^\circ$.



(a) Excited state



(b) Ground state

Figure 3.16: Wave functions of the ground and excited state, for 1 by 1 cell with Dirichlet boundary conditions, $\alpha = 60^\circ$, $B_{\text{ext}} = 25 \mathcal{E}_0 / (g\mu_B)$ and $a = 0.3$.

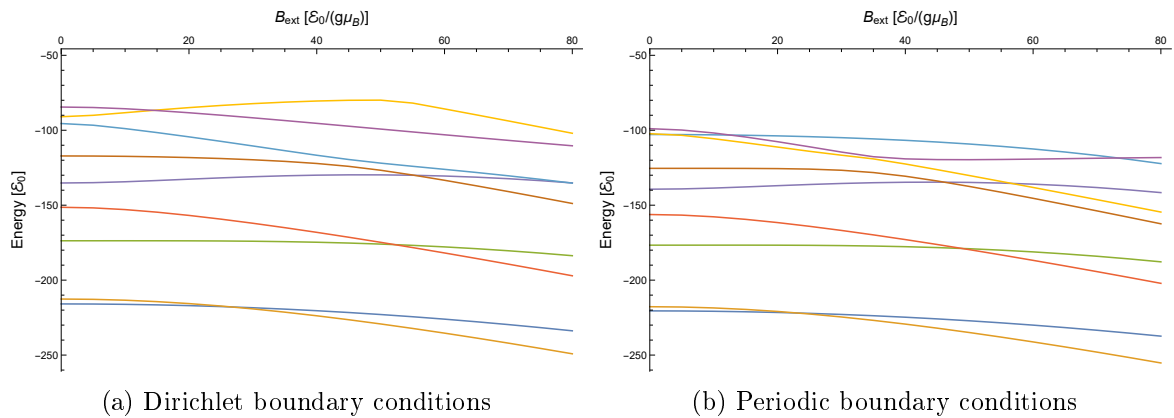


Figure 3.17: Energy levels of the first 9 eigenstates, as a function of B_{ext} , for $\alpha = 75^\circ$. Probably due to the potential being more shallow, state 7 does not appear to cross with states 8 and 9 (as it does in plots on Figures 3.9a and 3.13a)

3.5. Varying the shape of the lattice

Looking at the above examples, one can conclude there is little topological differences in the system's behavior between different values of α . However, quantitative analysis can be done by taking the angle α as an argument.

This work puts focus on the crossing between the first and second state, the plot on Figure 2.9 showed the relation between the crossing external magnetic field B_{cross} and the parameter a , which governs the strength of the potential. On Figure 3.18, a similar plot takes the angle α as the parameter and for $a = 0.3$ shows the obtained B_{cross} .

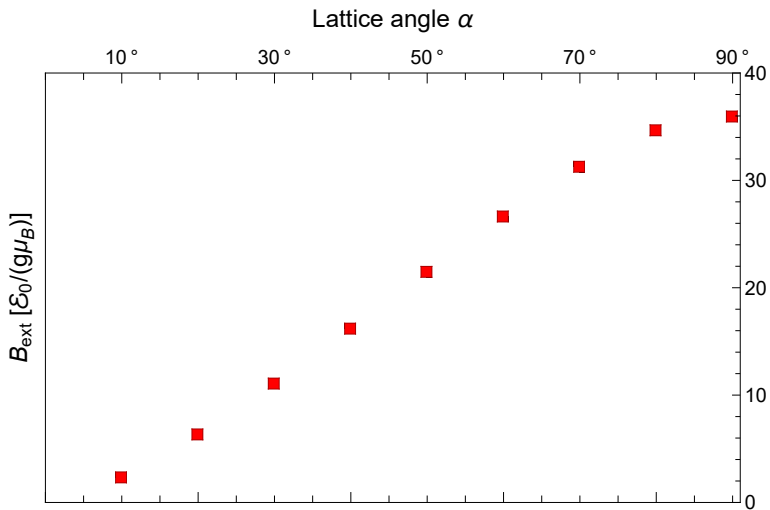


Figure 3.18: External magnetic field B_{cross} , at which the ground and excited state have the same energies, as a function of the lattice angle α . Dirichlet boundary conditions at the edges of a 1 by 1 elementary cell were applied. The square lattice ($\alpha = 90^\circ$) is represented on the right of the plot. To the left, lower angles are considered, down to 10° . For angles less than 45° or even 60° , the scalar potential resembles more a one dimensional lattice. However, even for angles as small as 10° , the crossing of the lowest two states can be observed and thus B_{cross} can be obtained (both for Dirichlet and periodic BC).

The B_{cross} value is important because it gives an idea about the scale of the system in terms of B_{ext} , for chosen parameters a and α . As mentioned previously and shown on figure 2.9, B_{cross} increases quadratically with a . As can be seen above, it appears to behave almost linearly with α , although at ranges investigated in this work ($\alpha \geq 60^\circ$) the relation is not as straightforward. The linear decrease in B_{cross} as α goes to 0° could either be the result of the change in potential shape or the cell's dimensions (at the border of which, Dirichlet BC are applied).

Apart from searching for B_{cross} at a given angle α , the B_{ext} can be kept constant, resulting in plots similar to those most frequently present in this work: Energy levels of the eigenstates, except with α instead of B_{ext} being on the horizontal axis. The choice of B_{ext} still remains and a somewhat distinguished choice is $B_{\text{ext}} = B_{\text{cross}}$. Such plots, for different values of a are displayed on Figure 3.19. Additional examples of similar plots, for $a = 0.3$ and B_{ext} both below and above B_{cross} are shown on Figure 3.20.

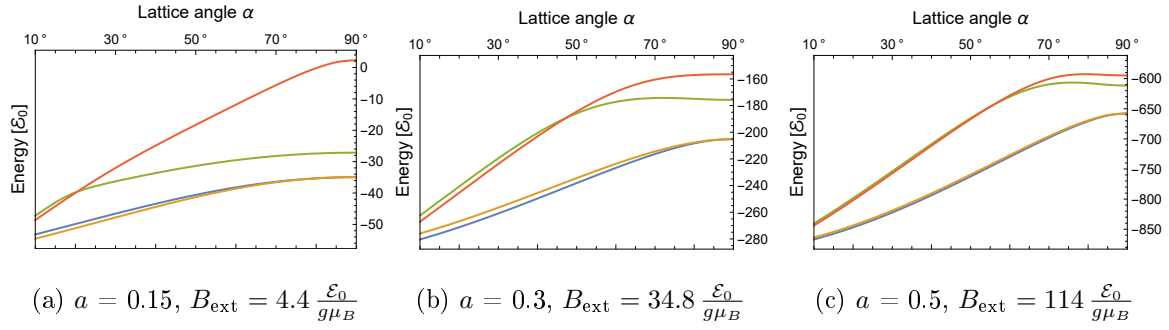
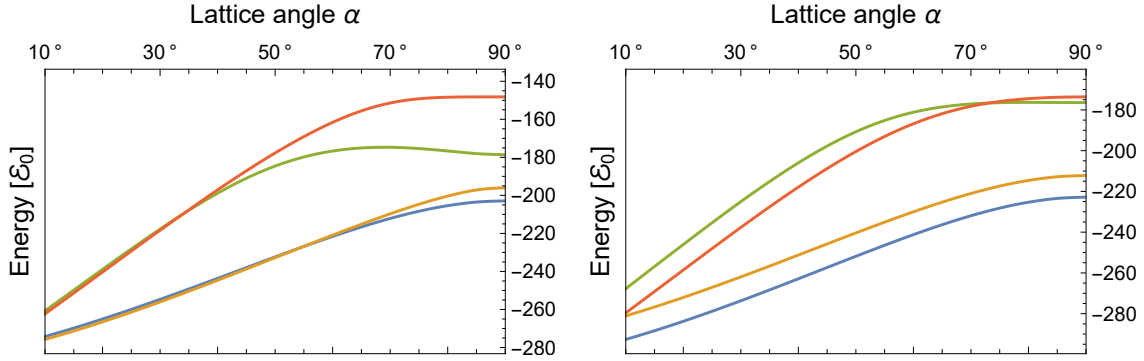


Figure 3.19: Energy levels of the first 4 states, as a function of the lattice angle α , Dirichlet boundary conditions. The B_{ext} was chosen to be equal to B_{cross} (calculated at $\alpha = 90^\circ$). Because of this the first and second state have the same energy at $\alpha = 90^\circ$, on the right side of the plot.



(a) $B_{\text{ext}} = 20 E_0/(g\mu_B)$, which is less than the B_{cross} at 90° . The first and second state cross at α around 50° . This means that $B_{\text{cross}}(a, \alpha) = 20 E_0/(g\mu_B)$ for $a = 0.3$ and α around 50° , which can be also seen on Figure 3.18.

(b) $B_{\text{ext}} = 60 E_0/(g\mu_B)$, which is more than the B_{cross} at 90° . The first and second state do not cross or rather — remain crossed, because 60 is above the $B_{\text{cross}}(a = 0.3, \alpha)$ for any α . 3.18.

Figure 3.20: Energy levels of the first 4 states, as a function of the lattice angle α , with $a = 0.3$ and Dirichlet boundary conditions. For this a , the B_{cross} at 90° is equal to 34.8

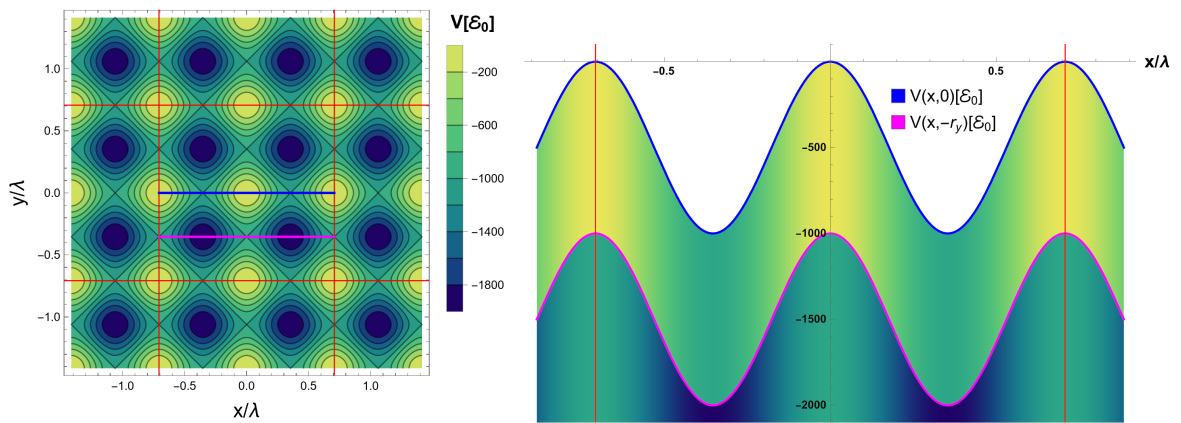
Chapter 4

2x2 Plaquette in square and rectangular lattices

Chapters 2 and 3 extensively explored the complexities of a 1 by 1 cell. The next step is to consider lattice cells composed of more than 1 elementary cell. However, the computational cost of calculating solutions grows cubically with the area considered. In this chapter, a 2 by 2 cell will be considered and while the solutions look similar, the system shows more complexity — most interestingly there appear differences between periodic and Dirichlet boundary conditions.

4.1. Square plaquette with periodic boundary conditions

Let's consider the potential arising from a lattice with $\alpha = 90^\circ$, shifted by (r_x, r_y) , so that the cell has symmetry around $(0, 0)$. A 2 by 2 cell will have boundary conditions along $\pm 2r_x$ and $\pm 2r_y$, as displayed on Figure 4.1a. First, periodic boundary conditions will be applied. Figure 4.1b demonstrates how the potential changes along $y = 0$ and $y = r_y$.



(a) Scalar potential as a function of x and y . In red are marked the edges of the 2x2 cell. Because of the change in lattice parity, the potential has a maximum at $(0, 0)$.
(b) Scalar potential at $y = 0$ (blue) and $y = -r_y$ (magenta). In red are marked the edges of the 2x2 cell. Because of the change in lattice parity, the potential has a maximum at $(0, 0)$.
conditions are applied.

Figure 4.1: Scalar potential in the lattice and periodic boundary conditions between 2 by 2 cells. The wave function will be localized in the four minima of the cell.

On Figure 4.2 the energies of the lowest 12 states are plotted as a function of B_{ext} . This is because, while the eigenstates in the 2 by 2 cell correspond to the ones in a 1 by 1 cell, there exist four corresponding states. The reason for this can be seen on Figure 4.3 which shows the obtained wave functions of the first eight states, out of which first 4 correspond to the ground state, and the 4 next to the excited state. Looking at the second component of the wave functions on Figure 4.3a, the 4 possible symmetries are noticeable. For a larger a value (parameter responsible for the strength of the potential), each set of four states appears degenerate, as seen on Figure 4.2a. This makes the plot similar to those seen in Chapter 2, such as the one on Figure 2.12a. Upon a closer look, or for a lower a parameter, it turns out only the second and third state are degenerate, which can be easily explained by looking back at Figure 4.3a — there is a symmetry of rotation by 90° , causing the degeneracy. This is demonstrated on Figure 4.2b, where three multiplets of 4 states are visible, with the middle two being degenerate.

Another important observation, although not so surprising is the crossing of the first 4 and next 4 states, similarly as it has happened between the first and second state for a 1 by 1 cell. This also happens for $a = 0.2$, however with less similarity, because of the lifted degeneracy. On Figure 4.4a energy levels for $a = 0.15$ are displayed, but the plot is not easily interpretable because some states appear crossed at $B_{\text{ext}} = 0$ already. Next to it, on Figure 4.4b is an extended version of the plot on Figure 4.2a, showing the first 36 states in the 2 by 2 cell. The large number of states poses problems to the state tracking algorithm, but similarities remain between this plot and the one on Figure 2.12c.

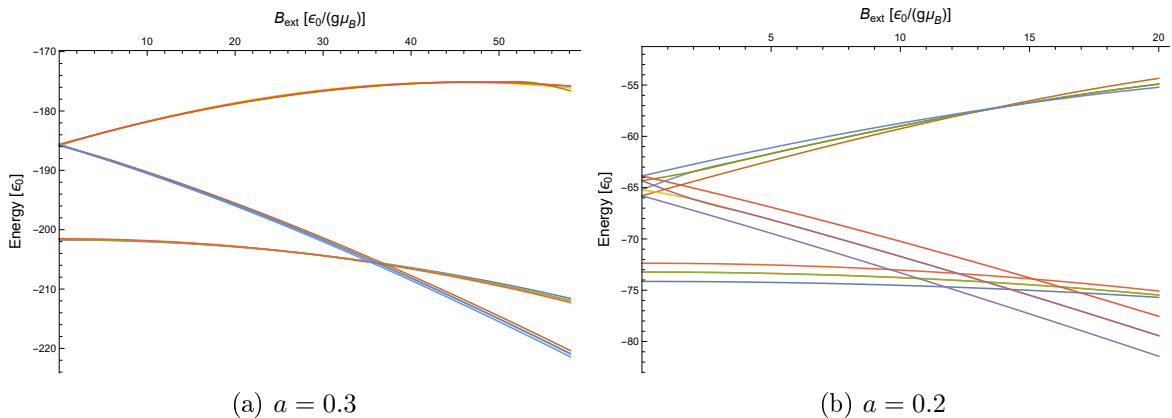


Figure 4.2: Energy levels of the first 12 eigenstates, as a function of B_{ext} in a 2 by 2 cell with periodic boundary conditions. For $a = 0.3$, the states appear degenerate, and the plot resembles the one obtained with a 1 by 1 cell. For $a = 0.2$ there is a noticeable difference between the lowest, highest and two degenerate states in each set of four. In both cases, the first four states cross the next 4.

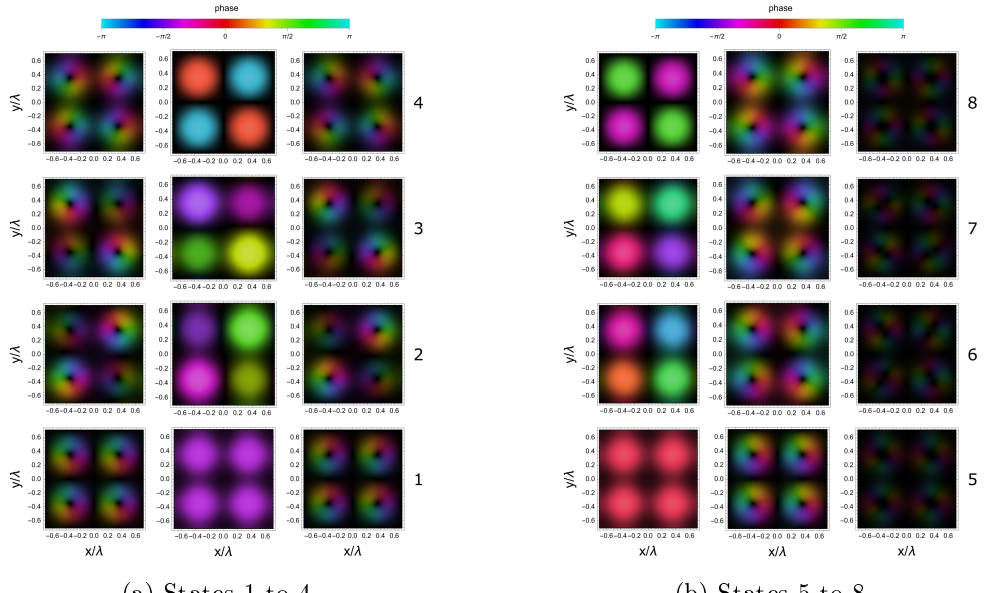
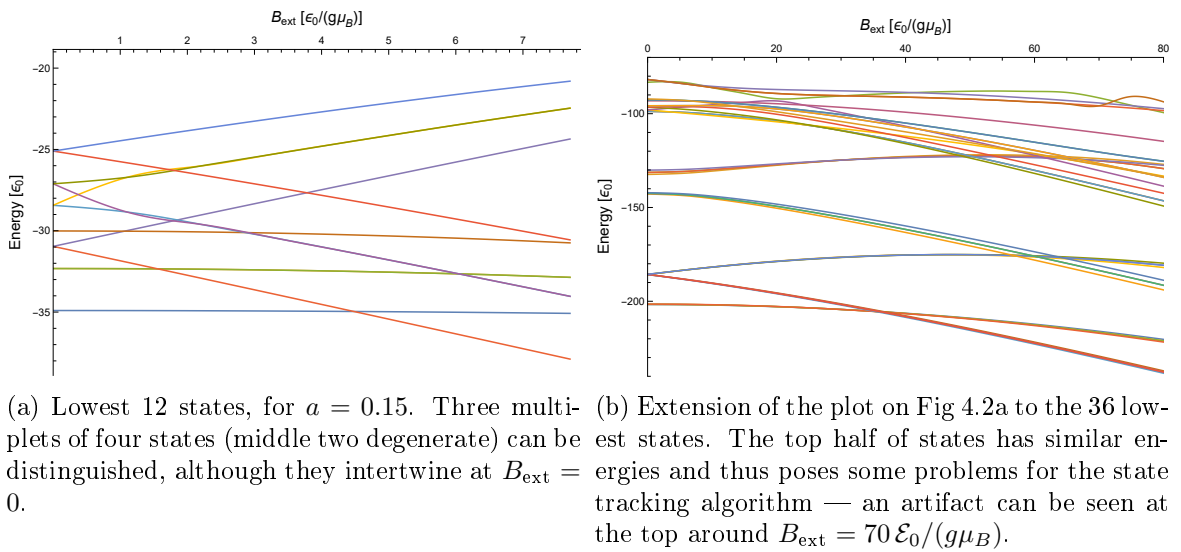


Figure 4.3: Wave function plots, for a 2 by 2 cell ($a = 0.2$, $B_{\text{ext}} = 5 \mathcal{E}_0/(g\mu_B)$), of the 4 lowest states (corresponding to the ground state in a 1 by 1 cell) and the subsequent 4 (corresponding to the excited state). In each set of four, the state with the lowest energy is displayed on the bottom. Hue represents the phase of the wave function, while the value of the color represents the modulus — brighter circles appear in the four minima of the scalar potential. Similarly to wave function plots in a 1 by 1 cell (such as on Fig 2.2) one of the components has constant phase in each minimum. It is in those components where the differences between states in a set are most apparent. There is rotational symmetry between the middle states, which causes degeneracy.



(a) Lowest 12 states, for $a = 0.15$. Three multiplets of four states (middle two degenerate) can be distinguished, although they intertwine at $B_{\text{ext}} = 4$.

(b) Extension of the plot on Fig 4.2a to the 36 low-lying states. The top half of states has similar energies and thus poses some problems for the state tracking algorithm — an artifact can be seen at the top around $B_{\text{ext}} = 70 \mathcal{E}_0/(g\mu_B)$.

Figure 4.4: Additional plots of energy levels as a function of B_{ext} in a 2 by 2 cell with periodic boundary conditions.

4.2. Square plaquette with Dirichlet boundary conditions

In this section of the work, the most interesting phenomena is observed. With the potential looking the same as on Figure 4.1, Dirichlet boundary conditions are applied on the 2 by 2 cell, as shown on Figure 4.5.

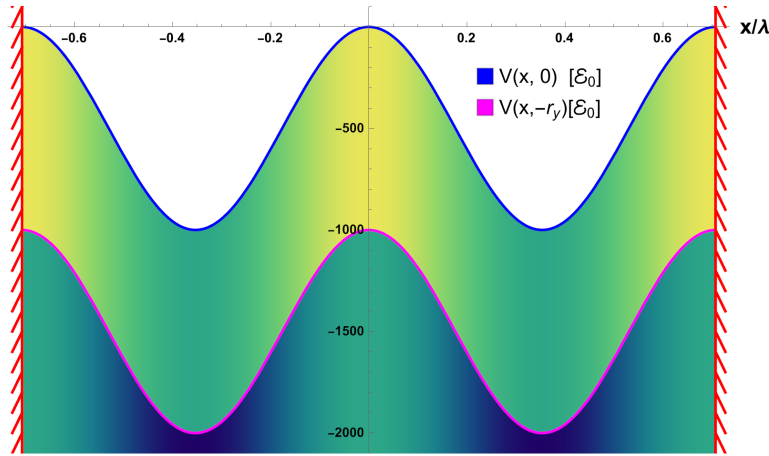


Figure 4.5: Scalar potential for a 2 by 2 cell at $y = 0$ (blue) and $y = -r_y$ (magenta), with Dirichlet boundary conditions marked on the plot.

The solutions are calculated for the exact same parameters as on Figure 4.2a, but with Dirichlet boundary conditions. On Figure 4.6a evolution of the states energies as a function of B_{ext} is displayed and surprisingly, the multiplets of 4 lower and middle states do not appear to cross. This phenomenon is described as avoided crossing, which appears between states of the same symmetry, for a Hamiltonian dependent on some parameter (such as B_{ext}) [6, 7]. In the case of $a = 0.3$ the states get very close to each other in the avoided crossing, and because calculating solutions for multiple B_{ext} is computationally expensive (and thus few of points are calculated), just looking at the energies would not be enough to detect the crossing. This is why it is crucial to track the states using the wave functions, as described in Chapter 5.

On Figure 4.7 wave functions of the four lowest states at B_{ext} lower, equal and larger than B_{cross} are displayed. Interestingly, there exists a noticeable transition of which wave function component has a constant phase (same color) per minimum — first it is the second component, then the first component. Similarly to the solutions for periodic BC displayed on Figure 4.3, except in the Dirichlet boundary conditions the states do not swap places, but *evolve* in a way that at $B_{\text{ext}} = B_{\text{cross}}$ neither of the solution components has constant phase. This evolution can be better seen on Figure 4.8, which follows the transition of a single state.

On Figure 4.6b another plot is made for $a = 0.2$. It shows that although the states are further apart in the multiplets, avoided crossing still occurs and is more noticeable because of a larger gap between the energies of state 4 and 5 at $B_{\text{ext}} = B_{\text{cross}}$. States 2 and 3, 6 and 7, as well as 10 and 11 are degenerate, as they were with periodic boundary conditions.

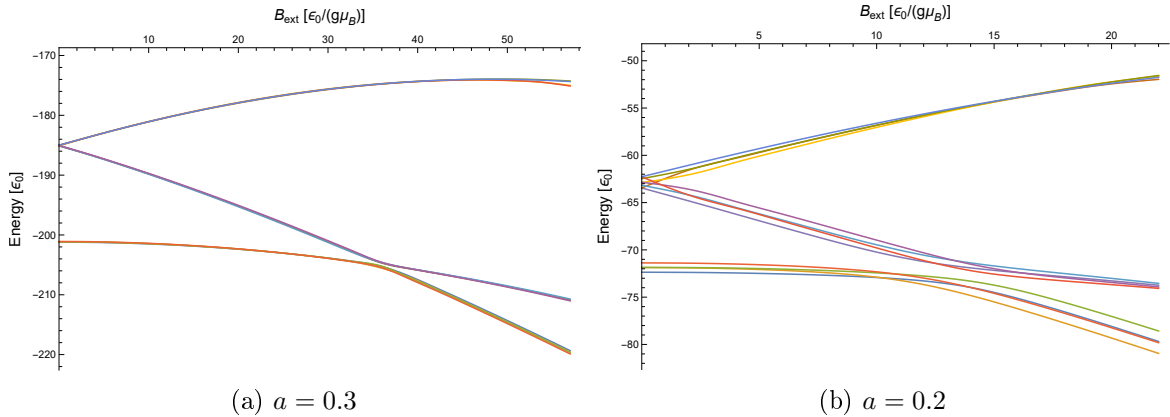


Figure 4.6: Energy levels of the first 12 eigenstates, as a function of B_{ext} in a 2 by 2 cell with Dirichlet boundary conditions. For $a = 0.3$ the plot looks similar to that with periodic BC, except the first four states avoid the next four. For $a = 0.2$ the states are further apart and the avoided crossing is even more apparent.

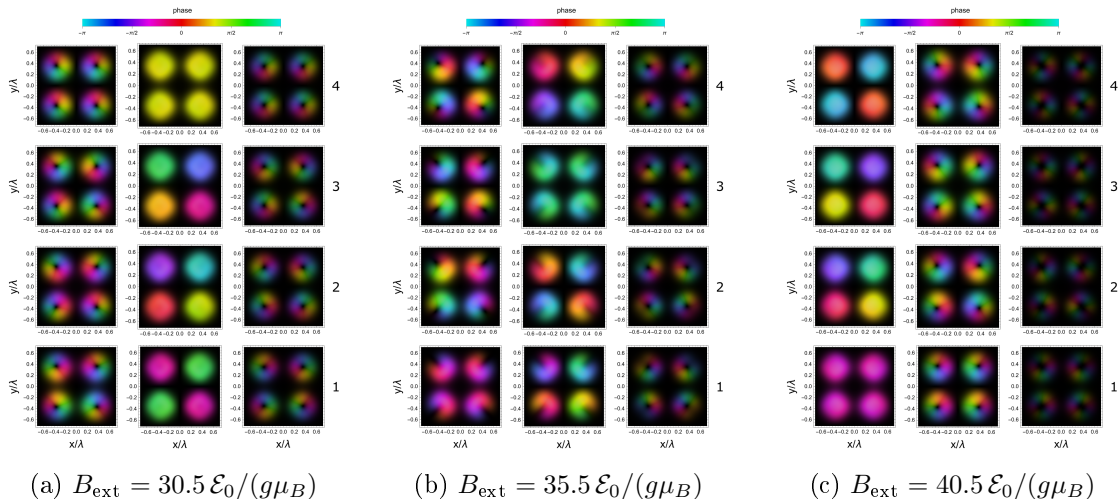


Figure 4.7: Wave functions of the four lowest states, in a 2 by 2 cell with Dirichlet boundary conditions. For $a = 0.3$, the external magnetic field of the crossing B_{cross} equals $35.5 \mathcal{E}_0/(g\mu_B)$. Wave functions of the states evolve: the distinct single color circles (meaning constant phase) appear initially in the 2nd and later in the 1st component of the wave function. The energies of the states change relatively, which means they swap places. For example, the first state appears to become the second state at $B_{\text{ext}} = 35.5 \mathcal{E}_0/(g\mu_B)$.

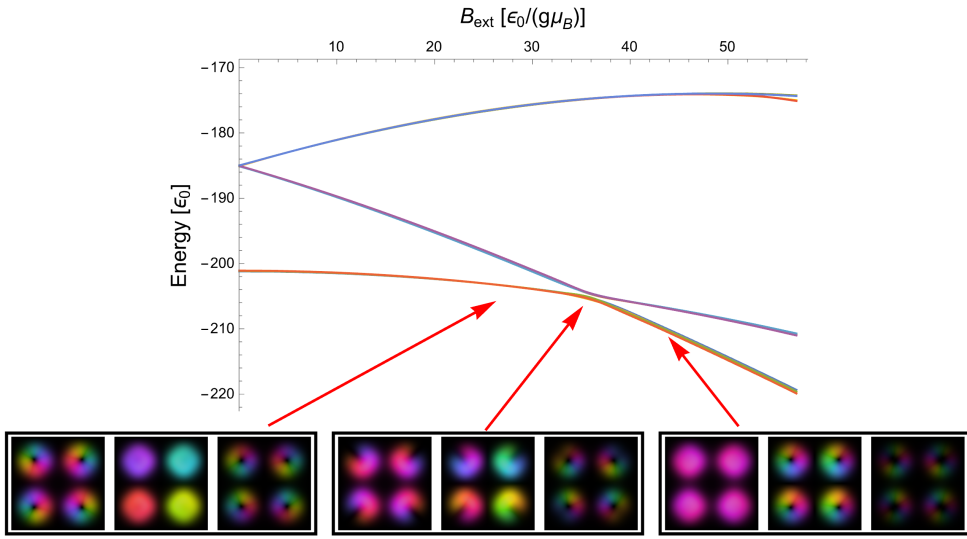
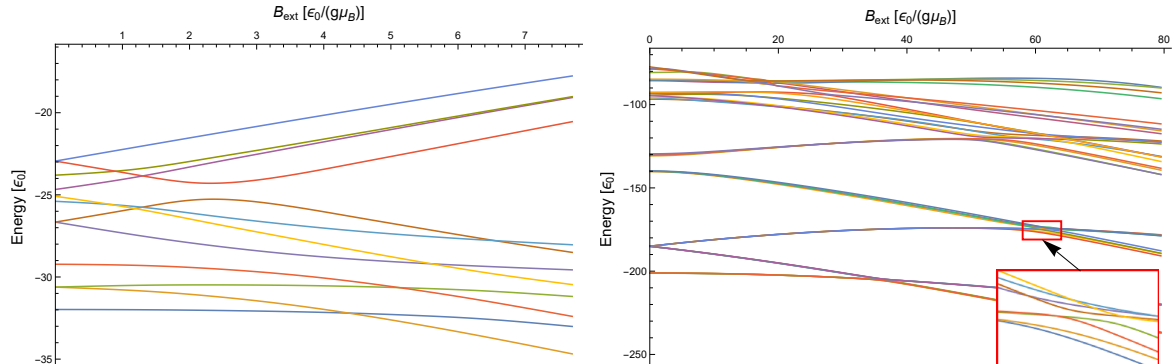


Figure 4.8: Evolution of one the states as B_{ext} is increased above B_{cross} . The wave function of the state was calculated at B_{ext} equal 30.5, 35.5 and 40.5[$\mathcal{E}_0/(g\mu_B)$]. Looking at the wave functions there are visible similarities between the second component at B_{ext} equal 30.5 and 35.5 as well as between the first component of 35.5 and 40.5[$\mathcal{E}_0/(g\mu_B)$].

As it turns out, the type of boundary conditions has an effect on the behavior of the system. In fact, some differences were present even in a 1 by 1 cell, as displayed on Figures 2.12c and 2.8. This however affected higher states, and in a 2 by 2 cell the bottom 8 states (corresponding to the ground and excited state of the 1 by 1 cell) show difference in behavior. This is perhaps the most interesting phenomenon documented in this work. The reason for this occurrence is not fully understood and the question of how the system would behave as the size of the lattice goes to infinity remains open.

On Figure 4.9a energy levels are plotted for $a = 0.15$ for comparison with Figure 4.4a. On Figure 4.9b a total of 36 states is plotted, and can be compared with Figure 4.4b. It appears that some higher states also exhibit avoided crossing.



(a) Lowest 12 states, for $a = 0.15$. Avoided crossing is present although not clearly visible.

(b) Extension of the plot on Fig 4.6a to the 36 lowest states. Upon closer inspection states 9 to 12 seem to avoid crossing with states 13 to 16.

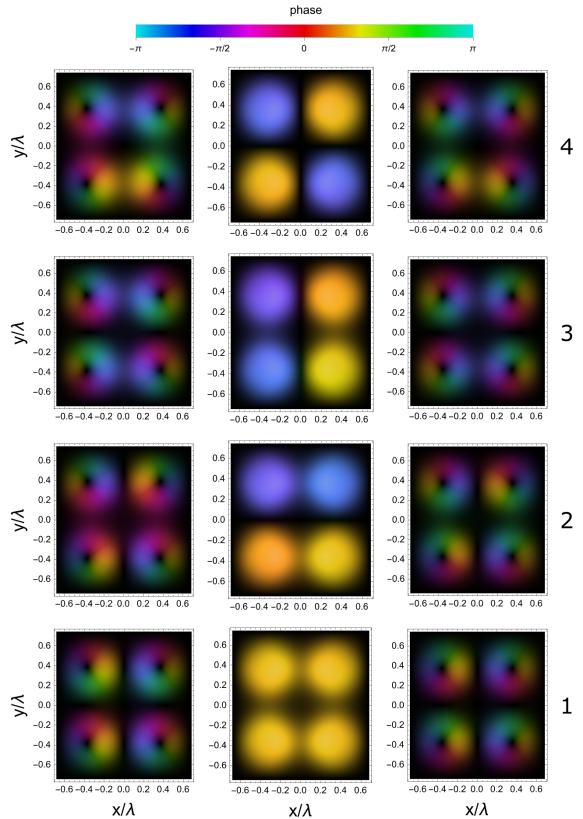
Figure 4.9: Additional plots of energy levels as a function of B_{ext} in a 2 by 2 cell with Dirichlet boundary conditions.

4.3. Rectangular plaquette

Two new phenomena were found by increasing the size of the cell: avoided crossing and the quadrupling into multiplets of four states, out of which the middle two are degenerate. Both of these serve as the motivation for implementing lattices with angle α less than 90° .

Avoided crossing is related to symmetry [6, 7], and thus could depend on the shape of the lattice. A lattice with $\alpha = 90^\circ$ has rotational symmetry of 90° , but for smaller α angles it loses that symmetry. This also lifts the degeneracy of the middle states: As demonstrated on Figure 4.10a, the two middle states *would* have symmetry, were it not for the elongation of the cell.

The effect of this can be seen on Figure 4.11b, where the energy of the states are plotted. The difference between the plot on Figure 4.2b demonstrates the effect of the change in α .



(a) Wave functions of the lowest 4 states for $a = 0.2$, $B_{\text{ext}} = 5 \mathcal{E}_0 / (g\mu_B)$, $\alpha = 85^\circ$ in a 2 by 2 cell with Dirichlet boundary conditions.

Below, plots of the lowest 12 energy levels as a function of B_{ext} are shown, for different boundary conditions and potential strengths ($a = 0.3$ and $a = 0.2$). The α angle is progressively decreased to 85° , 75° and 60° to demonstrate the changes in behavior in a rectangular cell.

Lattice at α equal 85 degrees

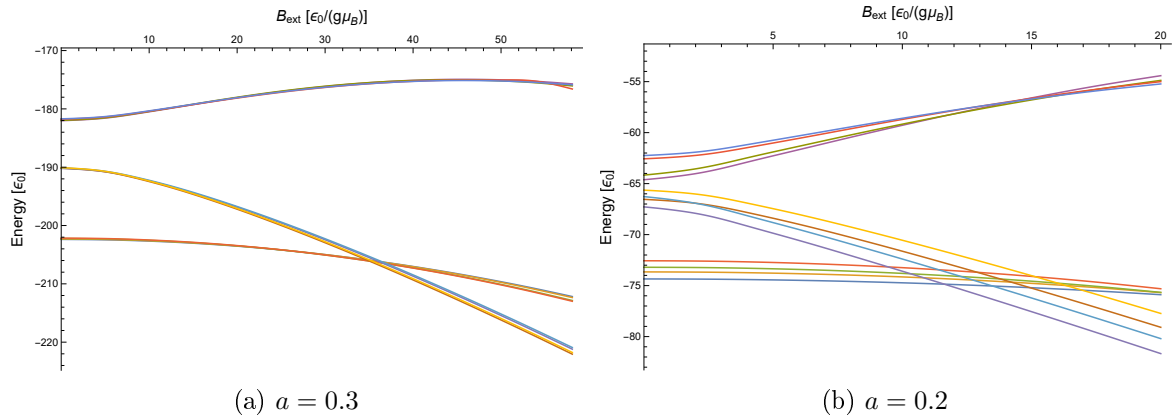


Figure 4.11: Energy levels as a function of B_{ext} in a 2 by 2 cell with periodic boundary conditions, for $\alpha = 85^\circ$.

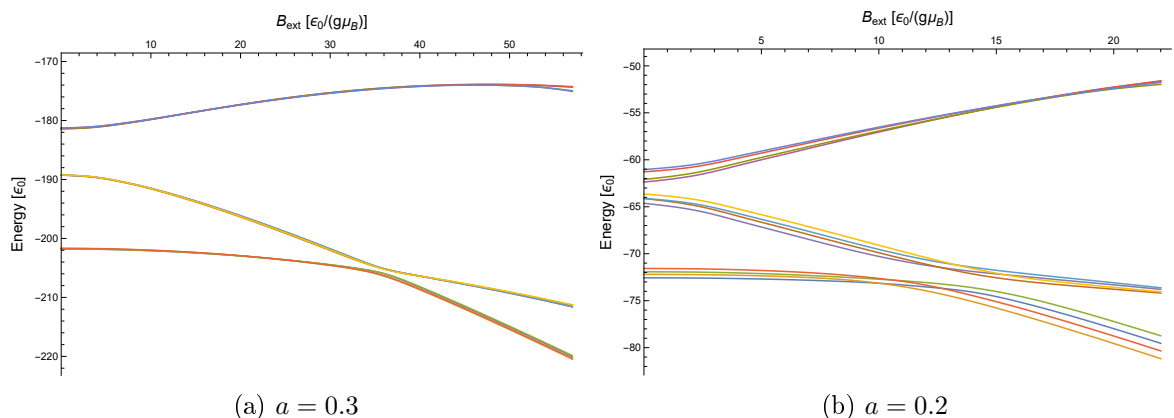


Figure 4.12: Energy levels as a function of B_{ext} in a 2 by 2 cell with Dirichlet boundary conditions, for $\alpha = 85^\circ$.

Lattice at α equal 75 degrees

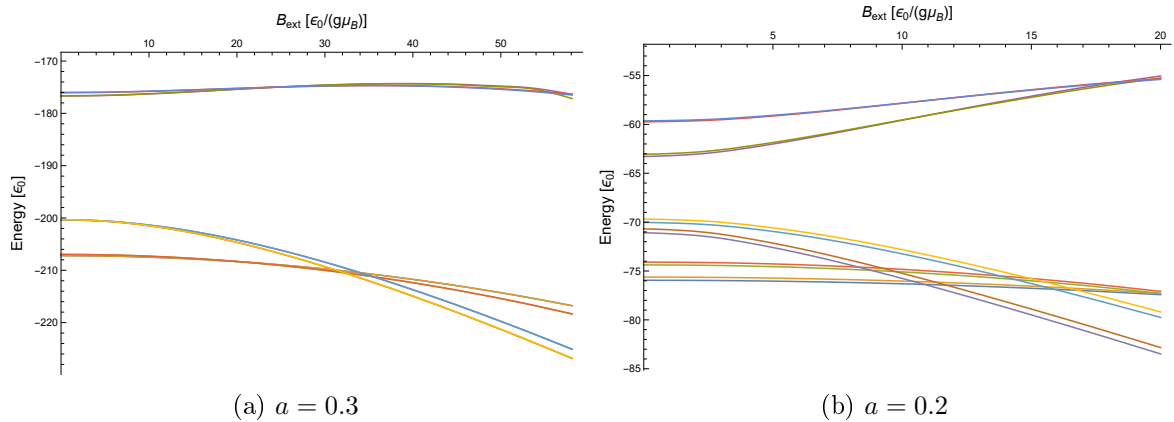


Figure 4.13: Energy levels as a function of B_{ext} in a 2 by 2 cell with periodic boundary conditions, for $\alpha = 75^\circ$.

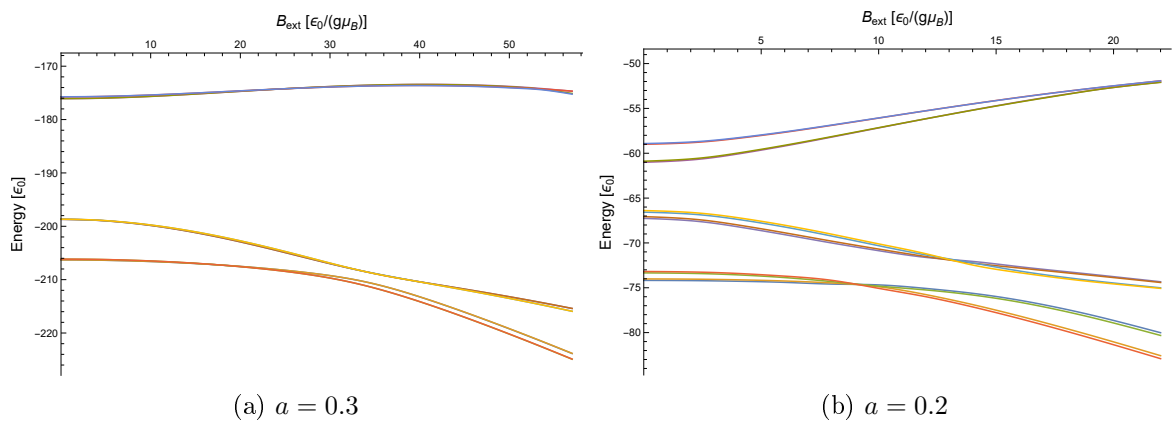


Figure 4.14: Energy levels as a function of B_{ext} in a 2 by 2 cell with Dirichlet boundary conditions, for $\alpha = 75^\circ$.

Lattice at α equal 60 degrees

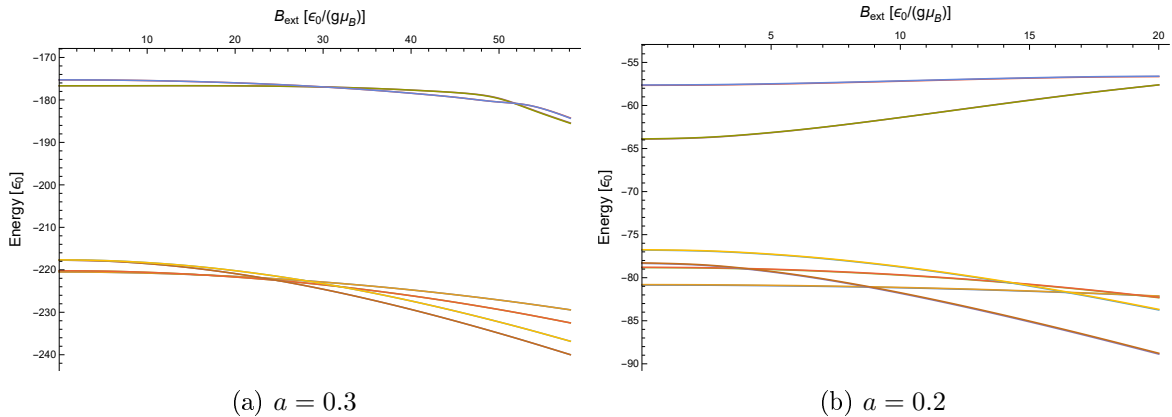


Figure 4.15: Energy levels as a function of B_{ext} in a 2 by 2 cell with periodic boundary conditions, for $\alpha = 60^\circ$.

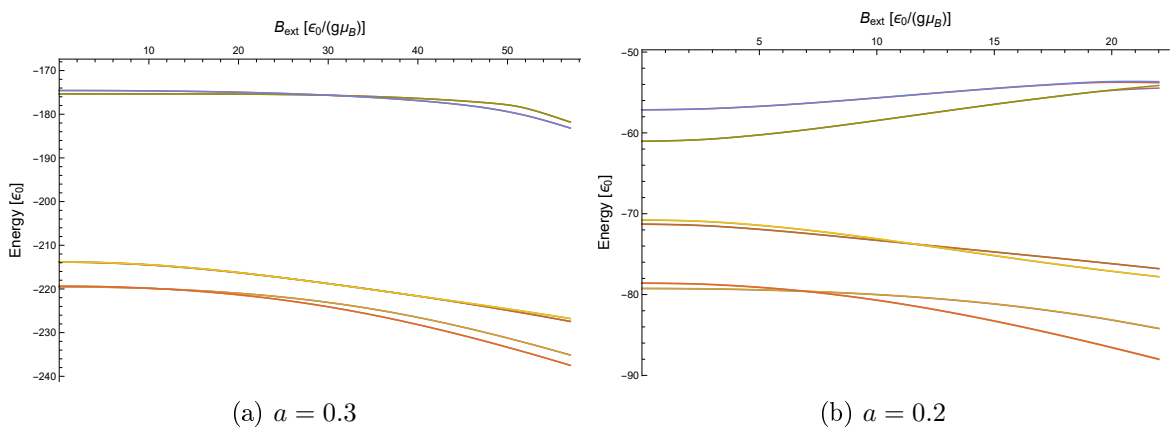


Figure 4.16: Energy levels as a function of B_{ext} in a 2 by 2 cell with Dirichlet boundary conditions, for $\alpha = 60^\circ$.

Effects of a rectangular cell

The plot on Figure 4.11a is very similar to that on Figure 3.7b. There exist multiplets of four states corresponding to each in the 1 by 1 cell, but the system behavior seems unchanged in the periodic BC case.

On Figure 4.12a we see that even for $\alpha < 90^\circ$ avoided crossing still occurs. Moreover, from Figures 4.14a and 4.16a we can conclude the gap between the states is even more prominent.

With a weaker potential ($a = 0.2$) the sets of states split, as it happened in the $\alpha = 90^\circ$ case. As can be seen on Figures 4.11b and 4.13b, the states are not degenerate (for reasons explained along Figure 4.10a). At smaller angles, this effect can be seen even for $a = 0.3$ (as seen on Figures 4.13a and 4.15a) however there the top two and bottom two states in each set appear degenerate. This suggests that the strength of the potential correlates with the gap between the lower and upper pair of states in each set, while the angle correlates with the gap between those pairs. Presumably this is because for large a and $\alpha = 90^\circ$ the states are localized in the four minima where the potential is isotropic, but for $\alpha < 90^\circ$ the vector potential (B_{fic}) is anisotropic even near the minima (Fig/ 3.5b).

Interestingly, in the case of avoided crossing, pairs of states in the multiplets appear to cross with one another, as demonstrated on Figures 4.12b, 4.14b and 4.16b.

4.4. Probability current

Another calculation that might be of interest is the visualization of probability currents. The probability current is calculated using the formula 4.1.

$$\mathbf{j} = \frac{\hbar}{M} \text{Im}(\Psi^* \nabla \Psi) \quad (4.1)$$

Direction and intensity of the current in the ground state of a 1 by 1 cell is shown on Figure 4.17:

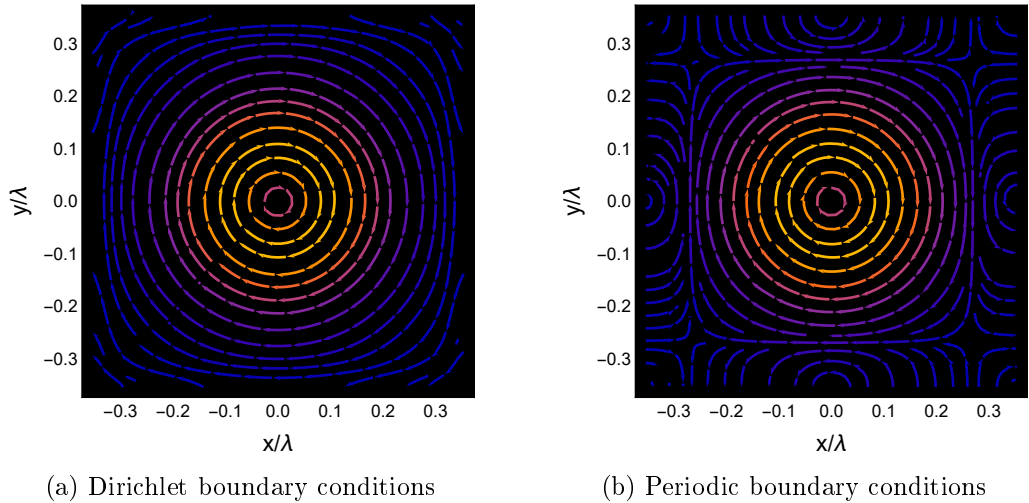


Figure 4.17: Probability current of the ground state in a 1 by 1 cell with $a = 0.3$ and $B_{\text{ext}} = 15 \mathcal{E}_0/(g\mu_B)$. The arrows indicate the direction of the flow, and the color represents the intensity of the current, which correlates to the magnitude of the wave function. The wave functions are localized in the center of the cell, however with periodic boundary conditions there is some flow through the cell boundaries.

Not much complexity can be found in the probability current in a 1 by 1 cell, except perhaps for the direction of the flow. Some complexity however, can be observed upon expanding the cell to a 2 by 2 cell. In a strong potential ($a = 0.3$), as expected, the wave function localizes in the four potential minima, which results in currents such as on Figure 4.18.

In weaker potentials however, some states exhibit current flow between the potential's minima, as displayed on Figure 4.19 which shows probability currents in the lowest 12 states of a 2 by 2 cell with Dirichlet boundary conditions and $a = 0.15$. This can lead to flow between the cells in the case of periodic boundary conditions, as shown on Figure 4.20. This further demonstrates why the type of boundary conditions has increased influence on the solutions for weaker potentials.

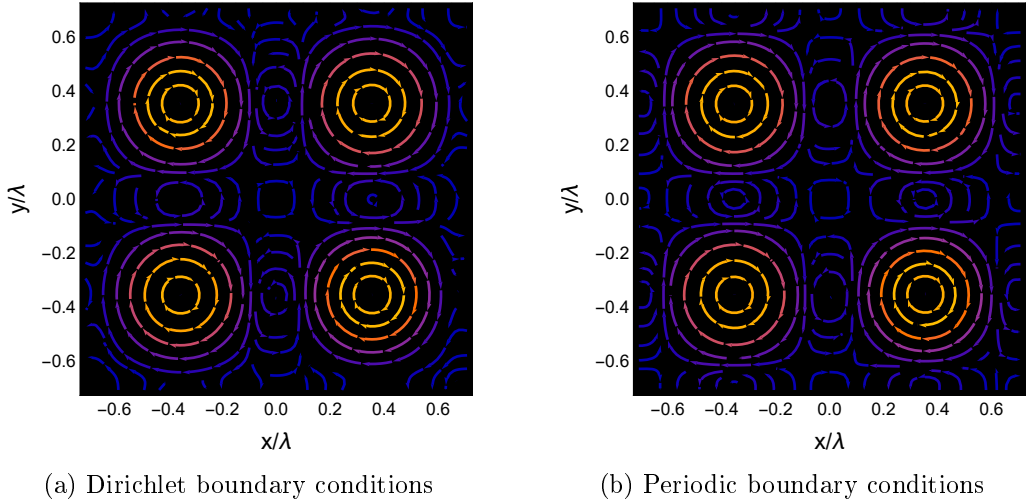


Figure 4.18: Probability current of the ground state in a 2 by 2 cell with $a = 0.3$ and $B_{\text{ext}} = 15 \mathcal{E}_0/(g\mu_B)$. The arrows indicate the direction of the flow, and the color represents the intensity of the current, which correlates to the magnitude of the wave function. The wave functions are localized in the four minima of the potential.

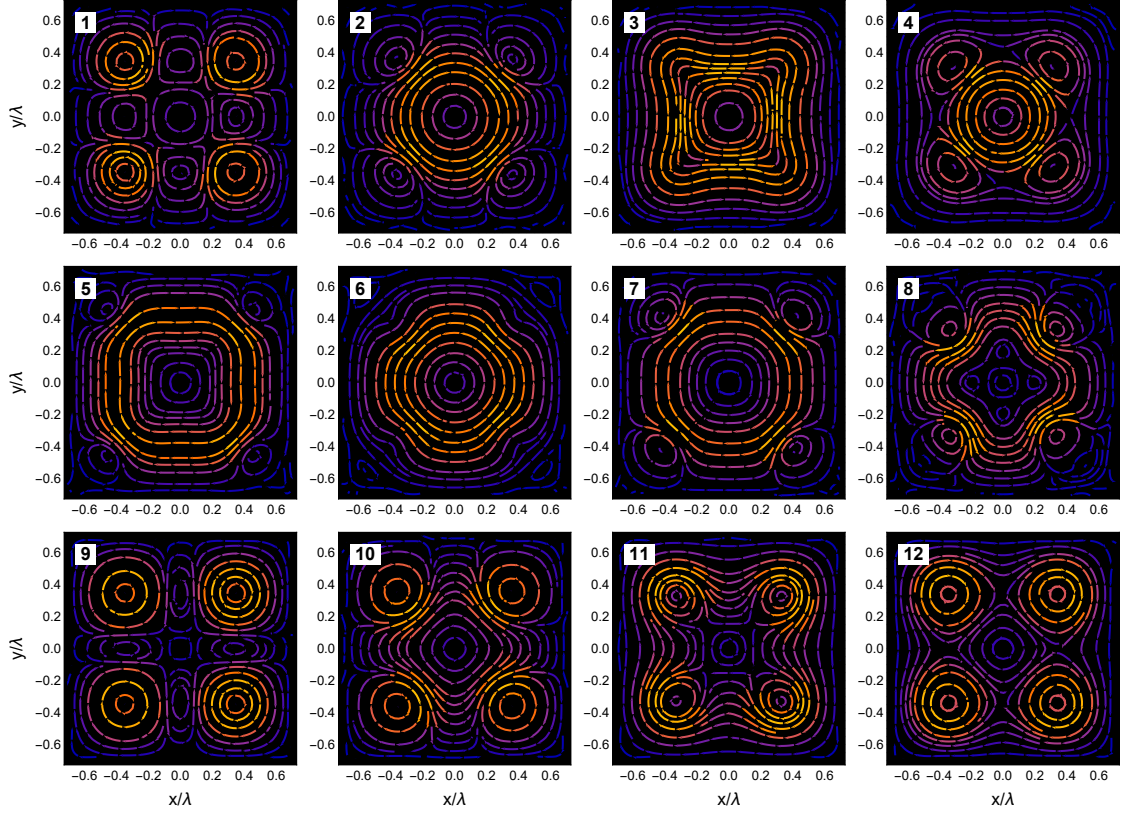


Figure 4.19: Probability currents in the lowest 12 states in a 2 by 2 cell with Dirichlet boundary conditions, $a = 0.15$ and $B_{\text{ext}} = 8 \mathcal{E}_0/(g\mu_B)$. Some states appear to have currents localized near the potential minima, while others have global currents in the cell. The parameters correspond to those on Figure 4.9a.

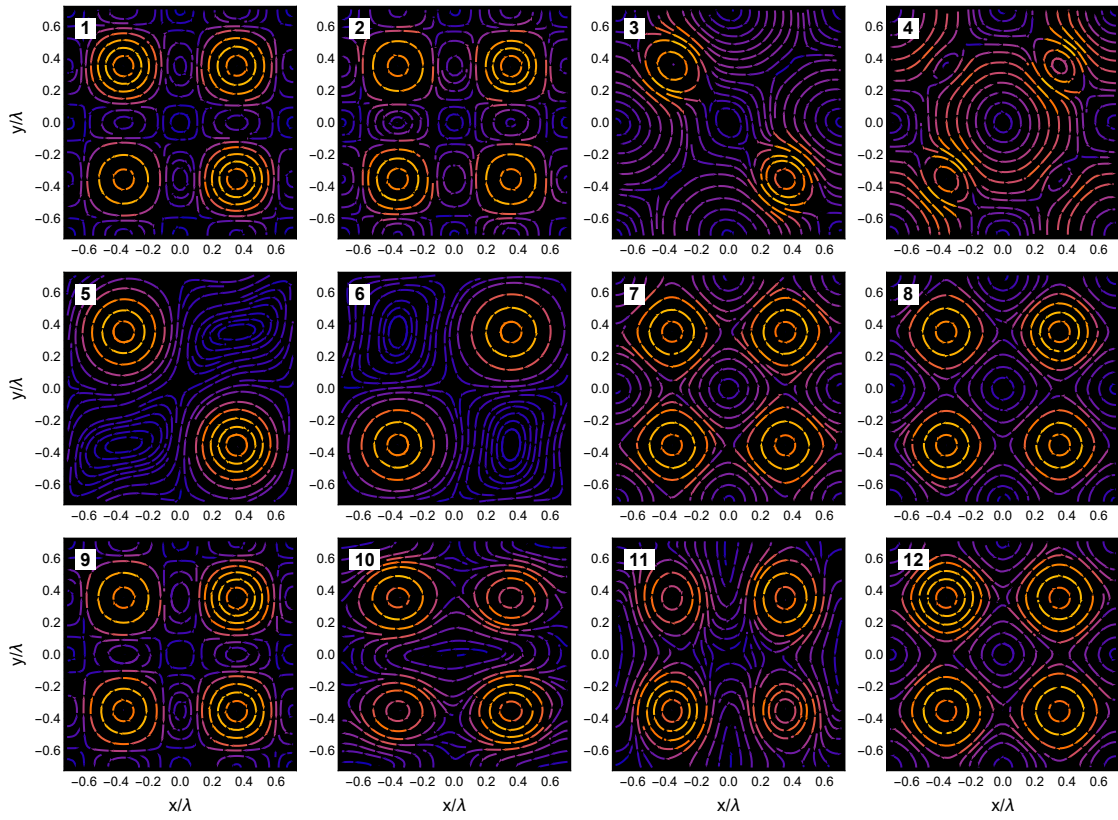


Figure 4.20: Probability currents in the lowest 12 states in a 2 by 2 cell with periodic boundary conditions, $a = 0.15$ and $B_{\text{ext}} = 8 \mathcal{E}_0 / (g\mu_B)$. Some states have probability currents localized in the four minima of the potential, some appear to have the largest current intensity near two of the four minima, while others have currents flowing through the periodic boundaries of the cell. Energies of these states are presented on Figure 4.4a.

In conclusion, probability currents are another way of visualizing the wave functions. Currents appear around the minima of the potential, but sometimes also appear globally in the cell. Although explored only briefly in this work, the existence of global currents (especially in relation with B_{ext}) is an interesting topic for further inquiries.

Chapter 5

Numerical solutions

The results for this work were obtained using Wolfram's *Mathematica* (Wolfram Research Inc., version 13.2), with code based on notebooks provided to me by the thesis supervisor. This chapter explains some technical details and shares some numerical methods used for this work.

5.1. Finding the eigenstates with *Mathematica*

This section will explain some technical details involved in obtaining the energies and wave functions of the system.

5.1.1. Derivation of the potential

First scalar and vector potentials need to be obtained. For that the $\mathbf{E}(x, y, z)$ vector is obtained, by summing four terms, each representing one laser beam. Two of the beams are counterpropagating along the x axis, and two along a line that forms an angle α with the x axis (by default, $\alpha = 90^\circ$). Each of the beams is polarized at 45° to the XY axis. Lastly, \mathbf{E} is rotated by an angle of $\alpha/2$, so that the lattice is aligned with both the x and y axis.

In the calculations, the wavelength is set to 1 and energies as well as magnetic fields are measured in \mathcal{E}_0 , which is $2\pi^2$ times the recoil energy. The scalar and vector potentials are calculated according to formulae 1.1 and 1.2, where I equals 1.5. The polarizabilities and electric field amplitudes are set to reflect the interaction between a ^{87}Rb atom with 70 W laser beams with a wavelength of 796, 456 nm. The relation between polarizabilities is set to $\alpha_1/\alpha_0 = 2$ (further scaled with the b parameter). This resulting potential parameters are $V_0 = 1000 \mathcal{E}_0$ and $B_0 = 500\sqrt{2} \mathcal{E}_0$ (applied in equations 1.3 and 1.4).

5.1.2. Solving the potential using *NDEigensystem*

Mathematica's *NDEigensystem* [8] is a powerful tool that allows to obtain eigenstates and eigenvalues numerically. Its power lies in the universality and applicability to symbolic expressions.

The operator for which eigenstates are sought is the Hamiltonian from equation 1.7:

$$\hat{H}(x, y) = -\frac{\hbar^2}{2M}\Delta + (V(x, y) - g\mu_B(\mathbf{B}_{\text{fic}}(x, y) + \mathbf{B}_{\text{ext}}) \cdot \mathbf{F}) \quad (5.1)$$

Parameters a and b are used to set the global and relative strengths of the scalar and vector potential. In this work $b = 2$ is used, and different a parameters between 0.15 and 0.3 are

explored.

Apart from implementing the potential, appropriate boundary conditions are applied at the edges of the cell. The edges of the cell are at $(\pm lr_x, \pm mr_y)$ for an l by m cell, where r_x and r_y are calculated according to the formula 3.1. The potentials are shifted accordingly (depending on the parity of l and m), so that the cell has symmetry around $(0, 0)$.

Additionally, in the case of the periodic boundary conditions (making use of Bloch's theorem) the form of the solution is assumed to be $\psi(\mathbf{r}) = e^{2\pi i \mathbf{k} \cdot \mathbf{r}/r_0} \mathbf{u}(\mathbf{r})$ (where r_0 would be the lattice periodicity). The x and y momentum: k_x and k_y are parameters of the solving function. Although not used in this work, solving with different types of boundary conditions at the horizontal and vertical boundaries of the cell is possible.

The *NDEigensystem* methods offers multiple options for the solver. For the results obtained in this work, a *FiniteElement* method was used, with a *MaxCellMeasure* (maximum mesh cell area) equal to 0.002. To obtain the eigenstates, the Arnoldi method [9] was used, with up to 10000 iterations. This method uses an estimation of the lowest energy level *shift* as input, which can be numerically estimated with a different method or approximated (using previously calculated points) by $-1.1B_{\text{ext}} - 3200 \cdot a^2 - 200$. The computational time required to calculate the solutions increases cubically as the number of mesh cells grows, directly correlating with the lattice cell's area. As a result, the calculations for the 2 by 2 cell take notably more time, approximately six times longer than those for a 1 by 1 cell. The number of calculated states is also specified, as it also correlates to the calculation time. For multiple values of B_{ext} solving can be easily parallelized with *ParallelTable*.

5.1.3. Analyzing the solutions

The results obtained are the energies and three components of interpolating functions for each of the n lowest states at a given B_{ext} , for set a and α . Because the wave functions are three-dimensional complex functions, no perfect way of visualization exists. Complex plots like on Figure 2.2 are useful for comparing states, and probability plots like on Figure 4.17 can help compress the three dimensions into one plot. Additionally, a spin projection plot can be made by calculating $\Psi^*(x, y)\hat{F}_i\Psi(x, y)$, where i is x, y or z .

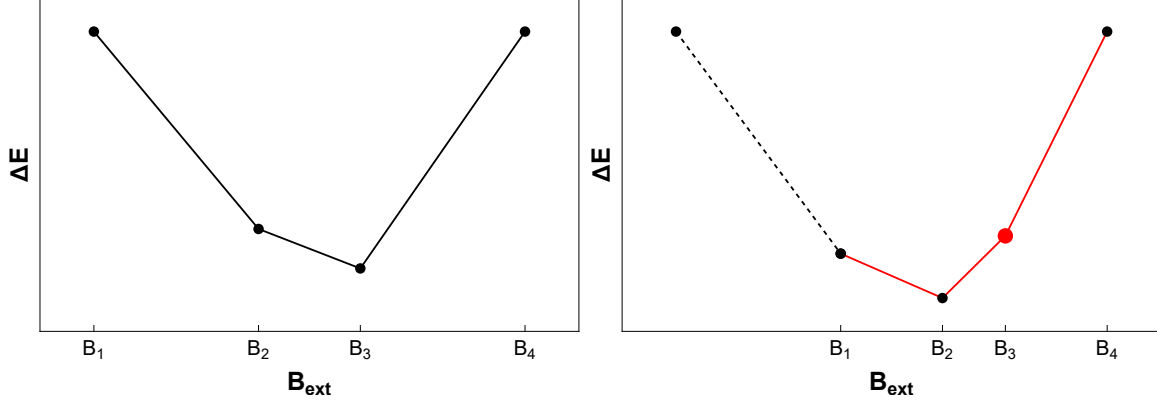
Finding B_{cross}

The external magnetic field at which the ground state has the same energy as the excited state — B_{cross} , is an important indicator of the scale at which the B_{ext} affects the energies. To make plots such as on Figure 2.9 and 3.18, an efficient way of obtaining B_{cross} is needed.

This can be treated as minimization problem, for the difference between the first two energies. Drawing inspiration from *Numerical Recipes* [10] the following algorithm is used:

- Find boundaries for the B_{cross} . Check $\Delta E(B_{\text{ext}} = 0) = |E_2 - E_1|$ and increase B_{ext} by a small ΔB_1 . Increase the B_{ext} with larger and larger increments: $\Delta B_{i+1} = \Phi \Delta B_i$ until the ΔE starts increasing (Φ is the golden ratio).
- Calculate an additional $\Delta E(B_3)$ to get 4 points, such as displayed on Figure 5.1a. The chosen B_i have the property that $(B_4 - B_1)/(B_2 - B_1) = (B_2 - B_1)/(B_3 - B_2) = \Phi$. The minimum is now certainly between B_1 and B_4 .
- Calculate the next point, either between B_1 and B_2 or B_3 and B_4 , depending on the relation between B_2 and B_3 , as shown on Figure 5.1b.
- Reassign B_i and repeat the previous step until $B_3 - B_2$ reaches expected precision.

- Return a final $B_{\text{cross}} = B_2 + (B_3 - B_2) \frac{\Delta E_2}{\Delta E_2 + \Delta E_3}$ (gaining additional precision from interpolation)



- (a) The minimum of $\Delta E(B)$ must lie between B_2 and B_3
(b) B_2 becomes B_1 , B_3 becomes B_2 and a new B_3 and B_4 (because $\Delta E(B_2) > \Delta E(B_3)$)
point is calculated.

Figure 5.1: Golden section search in one dimension [10], applied to finding B_{cross} at which the energies of the first two states are equal and thus $\Delta E = 0$. The ratio between the shorter middle segment and the longer side segments is the golden ratio Φ .

5.2. State tracking

Motivation

The main focus of this study lies on the energy levels of the eigenstates. Plotting them as a function of B_{ext} (and sometimes α) is the essential part of the work. Because data is obtained in sets for each B_{ext} , a problem emerges when trying to connect the points on the plot.

One solution would be to sort the states and connect them based on the ascending order of energy. This however wouldn't capture the phenomena of state crossing. Another option would be to use a tracking algorithm that extrapolates from initial seeding, detects when crossing occurs and sorts the data into states (similarly to how a seed tracking algorithm would work in a particle detector). This however requires frequent data points and runs into problems when narrow avoided crossing occurs, such as on Figure 4.6a — in that case an energy based tracking algorithm would most likely not detect the avoided crossing (see also Fig 5.2 and 5.3).

Solution

Fortunately, the interpolating functions obtained can act as a signature for which state, on the basis of which the states can be tracked. This is well explained on Figure 2.5. This method increases efficiency and requires less frequent points for correct tracking, but while robust it is not impervious. Because in the case of avoided crossing the states change the characteristic of the wave function (as demonstrated on Figure 4.8), only looking at the states before and after the crossing, the algorithm cannot correctly determine if the crossing was avoided or not. This can be mitigated by calculating additional points around the problematic B_{ext} .

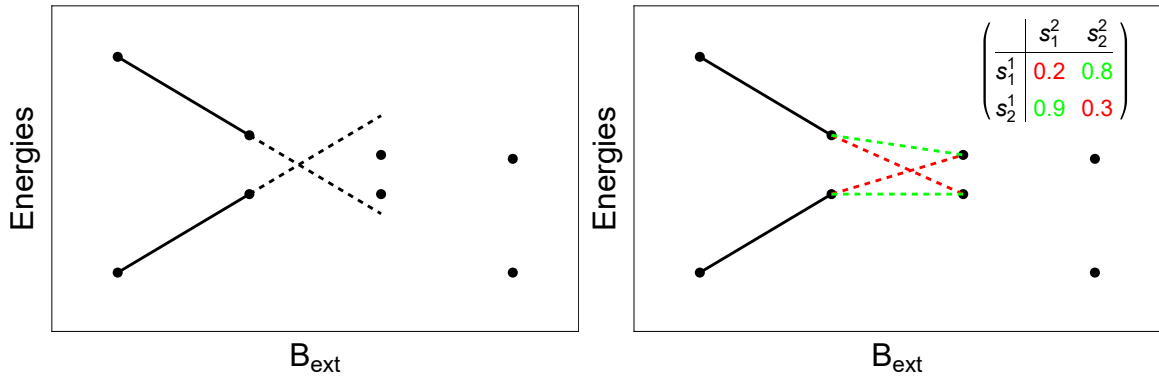
The proposed algorithm tracks the states as follows:

- For each of the n states, evaluate each of the three interpolating functions on an m by m grid. Flatten the results and store them in a vector \vec{s}_i^1 with m^2 complex values ($i \in 1, \dots, n$).
- Repeat the process for the solution at the next B_{ext} , obtaining a second list with n number of \vec{s}_j^2 vectors.
- For each possible pair of \vec{s}_i^1 and \vec{s}_j^2 vectors calculate the *Correlation* [11] between the vectors:

$$A_j^i = \text{Correlation}[\vec{s}_i^1, \vec{s}_j^2]$$
- Find the arrangement of states at the next B_{ext} which maximizes the sum of correlations between all the connected states. This corresponds to a problem known as the *balanced assignment problem* and can be solved quite efficiently [12].
- Repeat for the next value of B_{ext} .

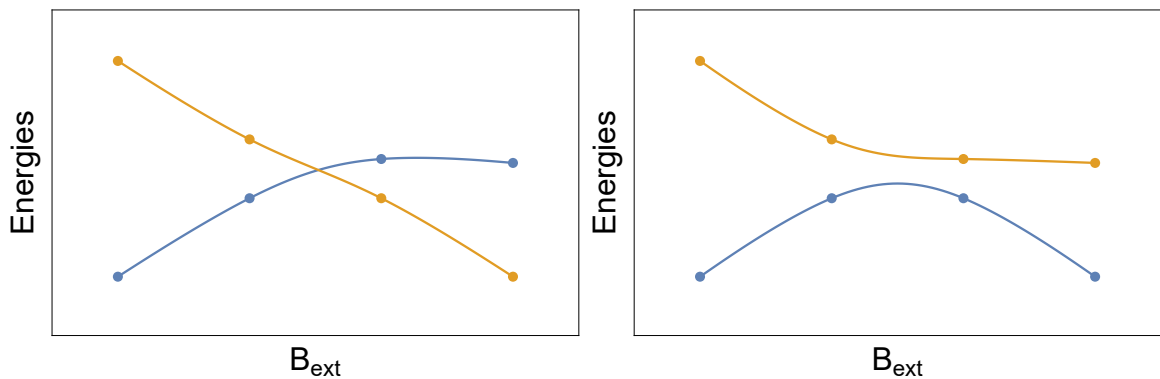
The correlation function is used, because the global phase can differ in corresponding solutions. This method requires evaluating the interpolating functions $3 \cdot n \cdot m^2$ times per each B_{ext} . Interestingly, the accuracy of the method does not increase with m , but works best for moderate values of m (around 10). This algorithm also requires calculating an n by n matrix and solving the assignment problem for each B_{ext} . The method can fail if the interval between B_{ext} is too large or for large values of n . Combining it with an energy based algorithm would improve both efficiency and accuracy.

A comparison between the energy based method, and the wave function method can be seen on Figure 5.2. Figure 5.2a shows how one can predict if a crossing has occurred by extrapolating the seeded function using data from last two points. On Figure 5.2b demonstrated is the way a wave function based tracking algorithm works, which is comparing all possible (n^2) connections between two sets of points and searching for an *assignment* that maximizes the sum. Figure 5.3 illustrates why a wave function based algorithm is necessary to capture the phenomena of avoided crossing.



- (a) An energy based algorithm extrapolates the function and sorts based on the order predicted at the next B_{ext} value.
- (b) A wave function based algorithm calculates signatures of all wave functions at two B_{ext} values, and selects an assignment that maximizes the sum (in this case, green).

Figure 5.2: Comparison between an energy and wave function based tracking algorithm. In some cases two algorithms might provide different results. In both cases the accuracy depends on the frequency of sampling.



(a) The energy based algorithm predicts a crossing (b) The wave function based algorithm predicts avoided crossing

Figure 5.3: Resulting plots from two algorithms presented at Figure 5.2. If two algorithms return conflicting results, the wave function based one is presumed to be accurate. However, an energy based algorithm can still be useful as it is more efficient for large n and can help eliminate obvious cases.

Chapter 6

Conclusions

6.1. Summary of results

Energy levels in a 2D spin dependent optical lattice were examined. Gaining inspiration from Ref. [2] and [3], a bosonic atom in a rectangular lattice was considered. A substantial effort was put into developing methods required for extensive analysis of the system's behavior throughout the parameter space.

Chapter 1 contains a short theoretical introduction to the topic of optical lattices examined in this work. In Chapter 2, a simple 1 by 1 square lattice cell was considered, and the results provided intuition of the system's behavior. In Chapter 3 the angle between the laser beams α is varied, and the effect of changes in both potential and cell size is examined. In Chapter 4 a 2 by 2 cell is considered. This chapter provides the most interesting result — difference in behavior between two boundary condition types. For any values of other parameters, a 2 by 2 cell with Dirichlet boundary conditions is shown to exhibit avoided crossing between the first two energy levels. Chapter 5 sheds light on the technical details of the numerical methods used, out of which the wave function based algorithm stands out for being surprisingly practical and accurate.

6.2. Implications and future work

The most important observations arising from the numerical calculations include:

- lifted degeneracy between the ground and excited state at $B_{\text{ext}} = 0$, in a 1 by 1 cell, upon changing the angle α
- lifted degeneracy between the middle two states in a set of four, in a 2 by 2 cell, upon changing the angle α
- avoided crossing between the lowest 2 states appears with Dirichlet boundary conditions, but only for cells larger than 1 by 1
- global probability currents appear in some states if the potential is shallow enough

The reason for the avoided crossing occurring only for some boundary condition types is not fully understood, and could be the subject of further inquiries. The topic of probability currents was mentioned briefly in this work and also provides opportunities for further investigations.

Acknowledgements

The author extends sincere gratitude to dr Grzegorz Łach and prof. Marek Trippenbach for providing him with this enriching opportunity. Their unwavering guidance and support have played a crucial role in shaping this thesis.

Bibliography

- [1] Oliver Morsch and Markus Oberthaler. Dynamics of Bose-Einstein condensates in optical lattices. *Reviews of Modern Physics*, 78(1):179, 2006.
- [2] P. Szulim, M. Trippenbach, Y. B. Band, M. Gajda, and M. Brewczyk. Atoms in a spin dependent optical potential: ground state topology and magnetization. *New Journal of Physics*, 24:033041, 2022.
- [3] Igor Kuzmenko, Mirosław Brewczyk, Grzegorz Łach, Marek Trippenbach, and Y. B. Band. Atoms in a spin-dependent optical lattice potential as a topological insulator with broken time-reversal symmetry, 2023. submitted to *Physical Review Letters*, arXiv:2308.07647.
- [4] F. Le Kien, P. Schneeweiss, and A. Rauschenbeutel. Dynamical polarizability of atoms in arbitrary light fields: general theory and application to cesium. *European Physical Journal D*, 67:92, 2013.
- [5] D. Jaksch. Optical lattices, ultracold atoms and quantum information processing. *Contemporary Physics*, 45(5):367–381, 2004.
- [6] J. von Neumann and E. Wigner. Über merkwürdige diskrete eigenwerte. *Phys. Z.*, 30:467, 1929.
- [7] L. D. Landau and E. M. Lifshitz. *Quantum Mechanics*. Pergamon Press, 1981.
- [8] **NDEigensystem**, *Mathematica*, Wolfram Research Inc.
<https://reference.wolfram.com/language/ref/NDEigensystem.html>.
- [9] W. E. Arnoldi. The principle of minimized iterations in the solution of the matrix eigenvalue problem. *Quarterly of Applied Mathematics*, 9:17–29, 1951.
- [10] William H. Press, Saul A. Teukolsky, William T. Vetterling, and Brian P. Flannery. *Numerical Recipes: The Art of Scientific Computing*. Cambridge University Press, 1992.
- [11] **NDEigensystem**, *Mathematica*, Wolfram Research Inc.
<https://reference.wolfram.com/language/ref/Correlation.html>.
- [12] Anurag Dutta, K. Lakshmanan, A. Ramamoorthy, Liton Chandra Voumik, John Harshith, and John Pravin Motha. A Review on Optimality Investigation Strategies for the Balanced Assignment Problem. *2023 International Conference on Computational Intelligence and Sustainable Engineering Solutions (CISES)*, pages 254–259, 2023.